DEGREE PROJECT

# The Crocodile Nose Connection

*Design and laboratory tests on a novel connection for structural hollow sections*

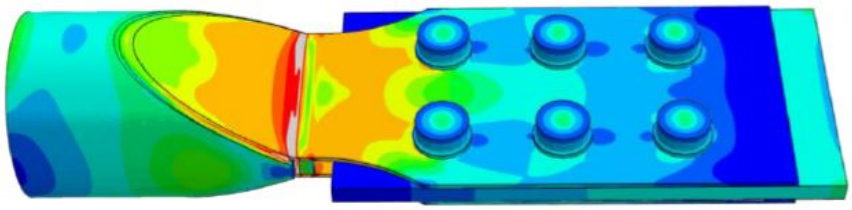

Kristoffer Öhman

**Civil Engineering, master's level**
**2018**

Luleå University of Technology
Department of Civil, Environmental and Natural Resources Engineering

LULEÅ UNIVERSITY OF TECHNOLOGY

# The Crocodile Nose Connection

# PREFACE

This thesis marks the end of the Master Programme in Civil Engineering at Luleå University of Technology. The tests performed in the thesis were conducted at the department of Civil, Environmental and Natural Resources at Luleå University of Technology, in the research group of steel structures at department of Structural Engineering. The tests were performed during the winter and the summer semester 2014/2015.

As a part of the HILONG project this thesis focus was to develop the acknowledgement of construction solutions for long span structures made by high strength steel. The connection is investigated by experimental tests both in laboratory and with finite element models.

I would like to thanks my examiner Professor Milan Veljkovic who has given me the chance to be a part of this project.

Also I would like to give a special thanks to my supervisor Panagiotis Manoleas who has given me a lot of new knowledge about steel structures. He has always been available during the project and because of that I am very grateful.

Last but not least I would like to thank my girlfriend Jasmina who has given me support during this time period.

Luleå, August 2015

Kristoffer Öhman

## ABSTRACT

The great properties and clear form makes the circular hollow section (CHS) appreciated by architects. When connecting these sections today it is common to use gusset plates. The knife-plate connection where the gusset plate is inserted into a slot made at the end of a circular section, is the most used connection today. This type of connections is not seen as aesthetically pleasing by architects because of its abrupt cut of the CHS.

An alternative for the knife-plate connection is the Crocodile nose connection (CN-connection). The benefits of the CN-connection is the absence of the abrupt cut and the protruding gusset plate, which makes it appreciated by architects. In this connection the CHS's ends are tapered, which creates two semi-elliptical cuts at both sides of the member. On these cuts, appropriate plates are fillet welded. These plates are shaped and bended so that when they are welded in place, the orientation of the extending part is parallel to the member axis. A gap is made between the extending parts so that a gusset plate can be inserted and bolted together with the member.

Four different specimens of the CN-connection are tested in order to find the best shape. Two specimens have a stiffener between the plates, at a small distance from the end of the CHS. The difference between the presence of a stiffener and the lack of it, is investigated. The results showed that the specimens with the connecting piece obtained a much higher ultimate load, up to 413 % higher. Two different angles of the CHS's cut is also investigated in order to see the most appropriate bevelling angle. In this case the results showed that the specimens with the smaller bevelling angle obtained a higher ultimate load, up to 40 % higher. A check of the weld connecting the plates and the CHS is also performed. This check was made with an assumed calculation model. The results showed that the calculation model only was valid for the specimens without the connecting piece. The calculation model must therefore be enhanced, in order to work for all dimensioning cases.

# ABSTRACT IN SWEDISH

De goda egenskaperna och den ideala formen gör det cirkulära tvärsnittet uppskattat av arkitekter. Vid anslutningar av dessa tvärsnitt är det idag vanligt att använda knutplåtar. Kniv-plåt-anslutningar där knutplåten förs in i en öppning i änden av det cirkulära tvärsnittet är det mest använda förbandet idag. På grund av rörets abrupta slut i detta förband är det inte estetiskt tilltalande enligt arkitekter.

Ett alternativ för kniv-plåt-förbandet är *Crocodile Nose*-förbandet (CN-förbandet). Fördelarna med CN-förbandet är frånvaron av det abrupta slutet och den utstickande knutplåten, vilket gör den uppskattad av arkitekter. I detta förband är det cirkulära tvärsnittets kanter nerfasade, vilket skapar två semielliptiska skärytor på båda sidor av röret. På dessa skärytor svetsas lämpliga plåtar med kälsvetsar. Plåtarna är formade på ett sådant sätt att när de är svetsas på plats är orienteringen av den utstickande delen parallel med rörets axel. Ett mellanrum mellan de utstickande delarna skapas så att knutplåten kan föras in och bultas fast tillsammans med röret.

Fyra olika provkroppar av CN-förbandet testas för att hitta den bästa utformningen. Två provkroppar har en avstyvning mellan plåtarna. Skillnaden mellan närvaron av avstyvningen och frånvaron av den är undersökt. Resultaten visade att provkropparna med avstyvningen fick en markant högre brottlast, upp till 413 % högre. För att även hitta den optimala vinkeln på skärytan har två olika vinklar undersökts. I detta fall visade resultaten att provkropparna med den mindre vinkeln gav en högre brottlast, upp till 40 % högre. Även en kontroll på svetsen som binder ihop plåtarna med röret är gjord. Denna kontroll gjordes med hjälp av en antagen beräkningsmodell. Resultatet visade att beräkningsmodellen endast är giltig för provkropparna utan avstyvningen. Beräkningsmodellen måste därför utvecklas, så den kan användas för samtliga dimensioneringsfall.

## ABBREVIATIONS

| | |
|---|---|
| CN | Crocodile nose |
| CNc | Crocodile nose connection |
| CHS | Circular hollow section |
| RHS | Rectangular hollow sections |
| SHS | Square hollow sections |
| HSS | High strength steel |
| FEA | Finite element analysis |
| FEM | Finite element method |
| BC | Boundary condition |

# CONTENTS

# 1 INRODUCTION

*The clear form and the excellent properties in compression and torsion makes the circular hollow section (CHS) appreciated by architects* [1]. *For visible parts in a structure the CHS is aesthetically pleasing due to the clean lines and closed section. These properties minimize the risk for dirt and corrosion* [2]. *The CHS has also been proven to be the best shape when it comes to resist loads from wind, water and waves* [3].

*One way to create connections with circular hollow sections is by using the crocodile nose connection* [4]. *This thesis focuses on the tensile behaviour of the joint. With the help of numerical simulations and laboratory tests the effect of stresses in the connection will be investigated, with the intention to validate hand calculations.*

*The laboratory tests and the numerical simulations concerning the CNc are performed as a part of the project High Strength Long Span Structures (HILONG). The HILONG project focuses on the development of higher strength steel grades for longer spans.*

## 1.1 Background

Due to their properties the hollow sections are widely applicable. Closed sections have a higher radius of gyration compared to open cross sections, which results in a much lower slenderness ratio. Another benefit of the hollow section is that the outer diameter can be the same even though the thickness is changed. In other sections, like the H-section, the outer diameter is changed with different thicknesses. Results of this can be a lower overall cost because of reduced beam fabrication and erection times [5].

The tubular shape has been known for its great properties for a long time. In the end of the 19$^{th}$ century larger dimensions of tubular sections were riveted together from rolled plates, simply because other methods were not available. A great example of this is the Firth of Forth bridge in Scotland [6].

In 1886 it became possible to roll short thick walled tubes thanks to the skew roll process, developed by the Mannesmann brothers. Some years later the pilger process was developed, and these two methods combined made it possible to fabricate longer thinner seamless hollow sections [6].

The Englishman James Whitehouse developed the forge welding of circular hollow sections and received patent in 1825 [7]. The welding process became more important in the 1930s when the American Fretz Moon developed the continuous welding process. After the Second World War the welding process had been more perfected and made it easy to weld hollow sections together [6].

## 1.2 Objectives and research questions

The purpose with the project is to investigate the crocodile nose connection in high strength steel, with and without connecting plate, see figure 1. Another aspect to be investigated is the bevelling angle, which affects the stress distribution in the welds that transfer the load from the plates to the CHS. These tests can later be a foundation in future research so that the connection can be constructed in the best possible way.

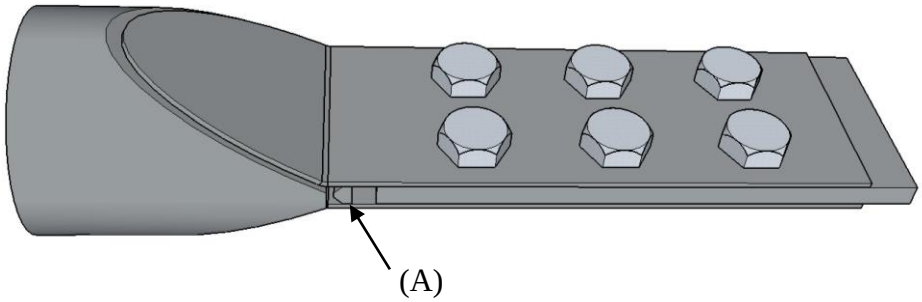


*Figure 1 (A) showing location of the connecting plate.*

Four different specimens are tested in this thesis. The goal is to find out more about the stress distribution in the area which is connecting the CHS with the inclined plates.

The research questions that are sought to be answered are summarized in the list below:

- What is the failure mechanism and the behaviour of the weld?
- What is the load capacity?
- What is the influence of the connecting plate?
- What is the influence of the bevelling angle?

## 1.3 Limitations

Two series of tests for the CN-connection are executed during the HILONG project: strength tests and long term tests. In the strength tests the focus is to explore the force-displacement curve and the ultimate load. During the long term test the loss of pretension force in the bolts are monitored in a period of 4 months. This report only considers the strength tests. The tests are performed in the laboratory facility, COMPLAB, at LTU.

Being a novel type of connection, literature is scarce. In order to define the strain measuring positions, simulations in Abaqus FEA is conducted prior the lab tests. Four of the test specimens are modelled, two with and two without the connecting piece. A static analysis under tension is thereafter conducted to provide an insight of the stress and strain flows in the connection. The results from the simulations are then used to accurately position the strain gauges. When the lab tests are completed, the results will be compared with the results from the FEA.

## 1.4 Scientific approach

The thesis is divided into three different parts in order to answer the research questions. First, literature is gathered to find the right material for the calculations and the computer simulations. Next step is to test the specimens both in the lab and with FEA. The four strength test specimens are modelled in Abaqus, simultaneously as the specimens are prepared and tested in the lab. The model can then be validated according to the results from the lab tests. A list of the different steps explained can be seen below:

1. A literature review is done in order to find similar tests of joints with the CHS.
2. Computer simulations using finite element models are executed with the software Abaqus.
3. The lab tests are performed on four different specimens of the CN-joint. The testing of the joints takes place at COMPLAB at LTU.
4. The different parts of the joint are hand calculated.
5. Result from the lab laboratory tests are then compared to the results obtained from Abaqus and the hand calculations.

## 1.5 Structure of the thesis

A summary of the chapters and the content is presented below.

*Chapter 1:* Outlines the content of the thesis, what the goals and what the methods used to achieve those goals are. The chapter also introduces the concept and the benefits of using circular hollow sections as structural members.

*Chapter 2:* The state of the art chapter, which explains the latest methods used in the design of steel structures.

*Chapter 3:* This chapter presents the properties for the parts used in the connection.

*Chapter 4:* Covers the hand calculation made for the connection, and the calculation methods featured in chapter 2.

*Chapter 5:* Considers the tensile test in Abaqus FEA. The different steps used in order to achieve the results are explained.

*Chapter 6:* Considers the tensile test in the lab. The assembly of the test specimens is explained step by step.

*Chapter 7:* The results obtained from chapter 4, 5 and 6 are presented.

*Chapter 8:* The results presented in the previous chapter are analysed. A comparison between the results from the FEA and the experimental tests is also performed in this chapter.

*Chapter 9:* In this chapter the results are discussed, as well as the improvements of the tests and future work.

*Chapter 10:* Considers the conclusions made from the results in the previous chapters. Results from the lab tests, FEA and hand calculations are compared.

# 2 STATE OF THE ART

*In this thesis the main focus is the design of a bolted and welded friction connection with a CHS member in high strength steel. The following paragraphs explain the basic design methods used nowadays for these connections. When constructing in steel it is important to know the resistance parameters for the used material. These parameters can be evaluated from results of tensile coupon tests. In order to answer the research questions addressed in section 1.2, the following topics considers the latest production, design and test methods.*

## 2.1 Steel production

In the CNc hot rolled plates are used. In hot rolling, an initial hot thick slab of steel is thinned down by a series of consecutive rolls to the desired thickness. When the work piece is compressed, the forces acting on the rolls will make them undergo a change in shape during the process. Elastic bending of the rolling tubes result in a work piece which is thicker at the centre and thinner on the edges. One way to avoid this problem when rolling is to make the diameter of the rolls larger at the centre than at the edges. The initial step is hot rolling, which is performed at a temperature higher than the recrystallization temperature of the metal. After hot rolling, steel gets a wrought structure with finer grains and enhanced ductility. [8]

## 2.2 Material testing

When designing in steel, the determination of the initial Young's Modulus, yield strength, ultimate strength and strains gives a solid foundation. The determination of these properties is in most cases done with an unaxial tensile coupon test, which is the most commonly used experimental method today [9]. The typical specimen used in tensile coupon tests has enlarged ends where the test machine is gripping the sample. In the middle of the specimen the cross sectional area will be smaller so that deformation and failure occurs there. Performed tensile tests should follow the rules explained in EN 10002-1 [10].

## 2.3 Connections with circular hollow sections

As a structural member the CHS is excellent to use in different kinds of constructions, such as buildings, towers, cranes and mechanical equipment [11]. When connecting tubular sections, the current rules in Europe for designing tubular structured joints under quasi static loading are covered in EN 1993-1-8 [12]. CHS as brace members are discussed in the CIDECT document [5] which covers welded connections with RHS in lattice tubular structures. Furthermore, [3] covers CHS as a truss member including discussions involving bolted connections. For the connections where gusset plates are attached onto the CHS and the flat-ended tubular section, design rules are given. Additionally, several connections with the CHS are discussed and design rules are given. All of the connections in the document ends however with the abrupt cut of the CHS, which is seen as un-appealing.

One of the easiest methods to connect CHS is with a slotted end knife-plate [1]. Gusset plates can be found in the majority of hollow section lattice structures. As hollow sections have become more popular due to their exceptional properties in compression and torsion, the combination of both gusset plates and hollow sections can be found in numerous applications [13]. Today the slotted end connection is the most popular where a plate is inserted and then welded to the CHS, as shown in figure 2 [14].

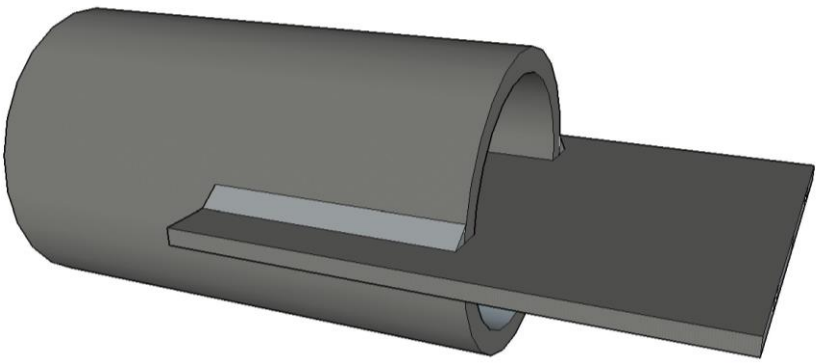

*Figure 2 The slotted end connection where the gusset plate is inserted into the slot.*

The most common failure mode when considering the slotted end connection is the circumferential tensile fracture (CF) and tear-out (TO) failure along the weld. When the CHS is slotted the whole section is not engaged in the connection and this can lead to a phenomenon called shear lag. The stress distribution in a cross-section of the joint is highly non-uniform. At the weld region along the slot, crack initiation can result in early failure of the tube material [13] [14].

The research of shear lag in tubular sections started in the early 1990s when British steel studied gusset plate connections in CHS and square hollow sections (SHS) [15]. Since then research in this area has been advancing, where the most recent is Willibald [16]. The main focus in that experiment was to study shear-lag induced tensile fracture of the hollow section. The report concludes that the shear lag effect can become critical in gusset plate connections. The largest effect on the connection was the connection length. The results also showed that large displacement can occur before failing, which is critical if there is a limit for the displacement. Another conclusion is that connections with slotted gusset plates, 3C, can reach premature failure due to deformations in the gusset plate. Therefore they should be avoided in compression connections.

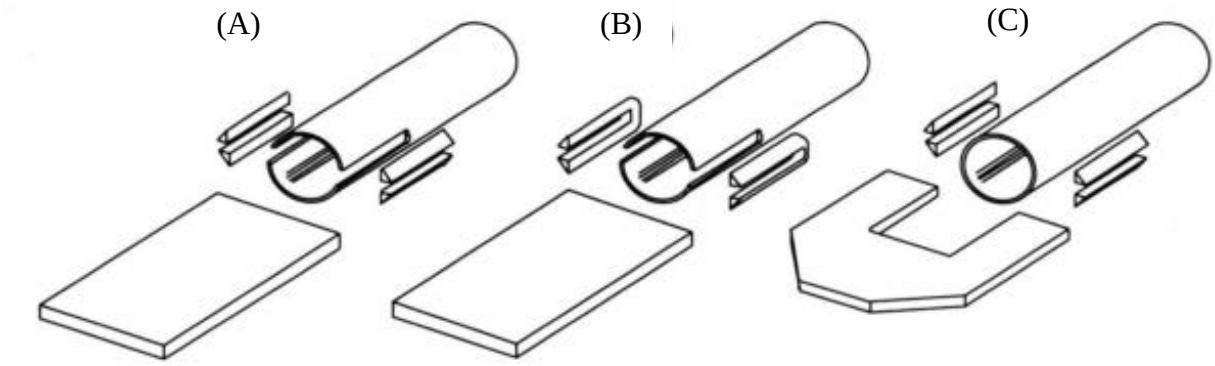


*Figure 3 Connection types investigated in* [16].

In an investigation by Ling the problem with shear lag failure in connections of very high strength steel, grades up to 1350 MPa, is addressed. Tests are conducted on 16 different test specimens and the results are compared with the design rules in USA, Canada and Australia [17].

## 2.4 Crocodile nose connections

As an alternative, the CN-joint can be used when connecting a CHS. The benefits with the CN-joint is the absence of the abrupt cut and the protruding gusset plate, which is seen by many architects as unappealing. When using this connection the CHS ends is tapered, creating two semi-elliptical cut off faces at both sides of the member. On these cut offs, appropriate plates are fillet welded. These plates are shaped and bended so that when they are welded in place, the orientation of the extending part is parallel to the member axis. A gap is made between the extending parts so that a gusset plate can be inserted and bolted together with the member. When the CHS is bolted to the gusset plate this secures the connection of the CHS to the other side without any eccentricity. Due to the design of the CN-connections it is relieved from the common shear lag problem leading

typical knife-plate connections in fracture [4]. The shape of the crocodile nose joint is shown in figure 4.

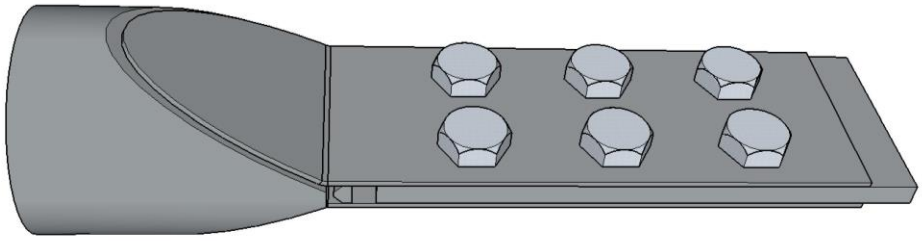

*Figure 4 Example of how the CN-joint can be designed.*

## 2.5 Design with high strength steel

The design with high strength steel is not yet fully covered in the Eurocodes. An addition to EN 1993 is part EN 1993-1-12 which extends the steel grades up to class S700 [18].

The use of high strength steel in steel structures has increased in over the recent years. Steel grade S355, which is one of the most used grades nowadays, was seen as high strength steel 25 years ago. Other industries are ahead of the construction industry when it concerns the use of HSS [19]. In the transport industry, where reduced weight, increased performance and safety are key factors, the use of HSS is exceptional. Steel manufactures can today, with help of continuous annealing, produce steel with a tensile strength up to 1400 MPa. Components using such high grades are especially safety related automotive components [20].

## 2.6 Design of bolted connections

Friction connections are used when gliding between the plates is unacceptable. One way to avoid this, and thereby create a friction connection, is to use high strength bolts which are pretensioned at 70% of the tensile strength. At this state, the faying surfaces are clamped together and their friction reacts to the load transferred from the member.

Section 3.4.1 and 3.4.2 in EN 1993-1-8 defines five different bolted connection categories, three describing shear connections and two describing tension connections. For the CN-connection, the load is transferred parallel to the member axis and the bolts are in shear. The connection is therefore counted as category C, which means that preloaded bolts in class 8.8 and 10.9 has to be used. The

design checks for the connection strength are found in table 3.2 in EN 1993-1-8 [12]. In the list below the required checks are summarized.

- Slip resistance
    - Friction coefficient
    - Pretension force
    - Number of faying surfaces
    - Number of bolts
- Bearing capacity
- Net cross-section
- Weld resistance

When calculating the slip resistance it is important to know the pretension force of the bolt and of the number of friction surfaces. The number of friction surfaces is dependent on the number of clamped plates, see figure 5.

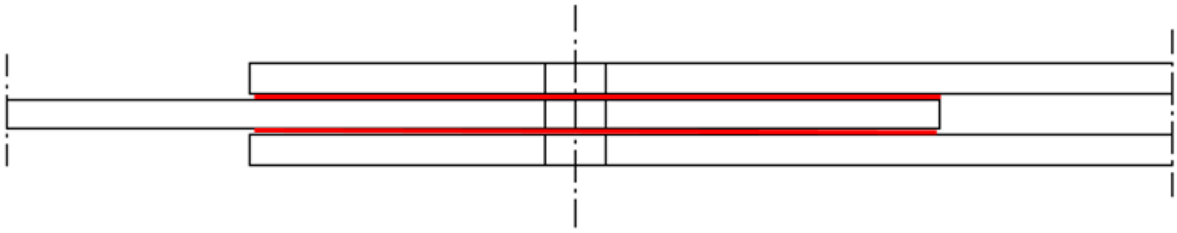

*Figure 5 Position of two friction surfaces in a connection with three plates. The friction surfaces are marked with red in the figure.*

In a slip resistant connection, an assessment of the friction between the clamped surfaces is crucial. In EN 1993-1-8 table 3.7, four slip factors are all located to different surface treatments [12].

## 2.7 Design of welded connections

When designing welds the weld material has to be equal to the welded steel grade. For the CN-connection, fillet welds are used. The fillet welds may be used when the fusion faces forms an angle between 60°and 120°. The angles are permitted to deviate from the given interval but in that case, different design approaches has to be used. If the weld is smaller than 60° it should be considered to be a partial penetration butt weld. If the weld is greater than 120° it should be tested in accordance with EN 1990 Annex D [12].

The fillet weld is seen as the largest triangle that can be inscribed within the fusion faces and the surface of the weld. The effective throat thickness, a, is measured perpendicular to the outer side of the triangle, see figure 6, and should at least be 3 mm [12].

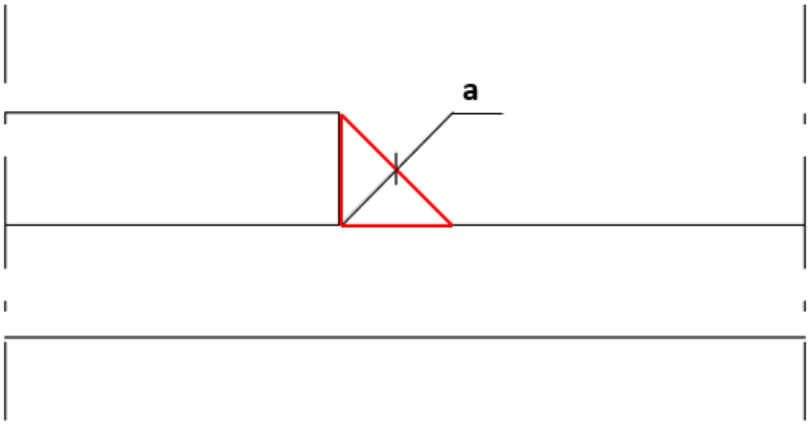


*Figure 6 Measurement of the effective throat thickness, a. The weld is marked with red.*

For the determination of the design resistance of a fillet the Eurocode describes two methods

- Directional method
- Simplified method

The directional method resolves the forces transmitted by a unit length of weld into components parallel and perpendicular to the longitudinal axis of the weld and normal and perpendicular to its throat [12].

In the simplified method the design resistance of the weld is assumed to be adequate. If this method is to be used the following criteria must be satisfied [12]

$F_{w,Ed} \leq F_{w,Rd}$

where

$F_{w,Ed}$ is the design value of the weld force per unit length

$F_{w,Rd}$ is the design weld resistance per unit length

## 2.8 Design of friction connections

In a friction connection the load is completely transferred by the frictional resistance on the contact surface. The frictional resistance contributing factors are the bolt preload and the slip resistance on the contact surfaces. In a slip-resistant connection, there will be no slip during the serviceability. In structures where slip is not acceptable, and can lead to unwanted deformations, a slip-resistant connection is appropriate. The load applied in a slip-resistant connection usually acts on a plane that is perpendicular to the fasteners axis. When the frictional resistance has been exceeded and slip occurs the plates will go into bearing with the bolts. This point is assumed to be the maximum capacity for a slip-resistant joint [21]. The design of slip resistance should be calculated according to [12]. In slip-resistant connection the value achieved from the Eurocodes can be regarded as the ultimate limit state [22].

# 3 SPECIMEN DESCRIPTION

## 3.1 Part inventory

Both the experimental tests and the FEA consists of four different specimens. The parts which are included in all of the specimens are the inclined plates, gusset plates, CHS, bolts, washers, nuts and two semi-elliptical welds. There is also a stiffener known as the connecting piece present in two of the specimens. Table 1 shows an inventory of all the parts.

*Table 1 Part inventory for the specimens. Values in parenthesis are for the lab tests.*

| Part | CN 1 | CN 2 | CN 3 | CN 4 |
|---|---|---|---|---|
| **Inclined plate** | 2 | 2 | 2 | 2 |
| **Gusset plate** | 1 (2) | 1 (2) | 1 (2) | 1 (2) |
| **CHS** | 1 | 1 | 1 | 1 |
| **Bolt** | 6 | 6 | 6 | 6 |
| **Washer** | 12 | 12 | 12 | 12 |
| **Nut** | 6 | 6 | 6 | 6 |
| **Connecting piece** | 1 | - | 1 | - |

.

## 3.2 Tube and plates

The experimental study consists of four different test specimens that are tested in tension. Each of the specimens are designed with different fabrication details. Figure 7 and 8 shows the dimensions for the inclined plates, while table 2 shows the dimensions on the CHS. The tubes in the tests are all of steel grade S690 and delivered by Vallourec. The plates are fabricated by RUUKKI and are a thermomechanically rolled, class M, cold formable, class C, structural steel which meets and exceeds the requirements of EN 10149-2 [23]. The plates, which are of steel grade S650, have previously been tested in a tensile test to achieve more specific material properties. Six different parts of the plates were tested according to the procedure described in [10]. Data from these tests are presented in annex A. The fillet welds connecting the CHS and the inclined plates are designed with a thickness of 4 mm.

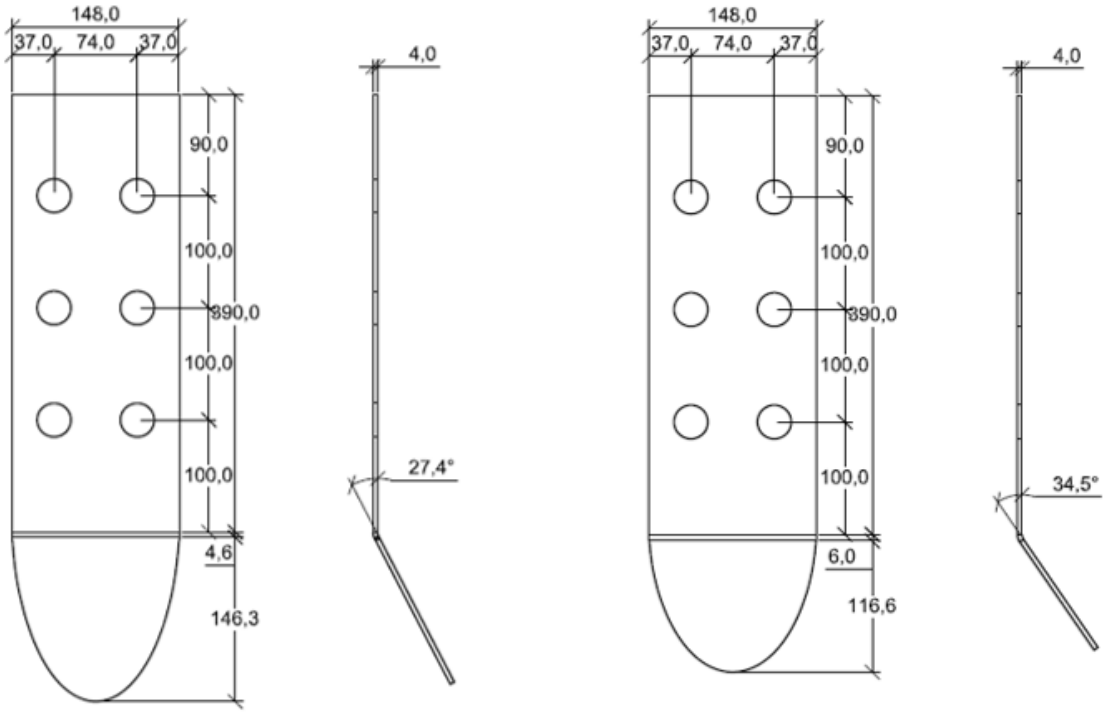


CN 2 CN 4

*Figure 7 Dimensions of the inclined plates without the connecting plate. Units in millimetres.*

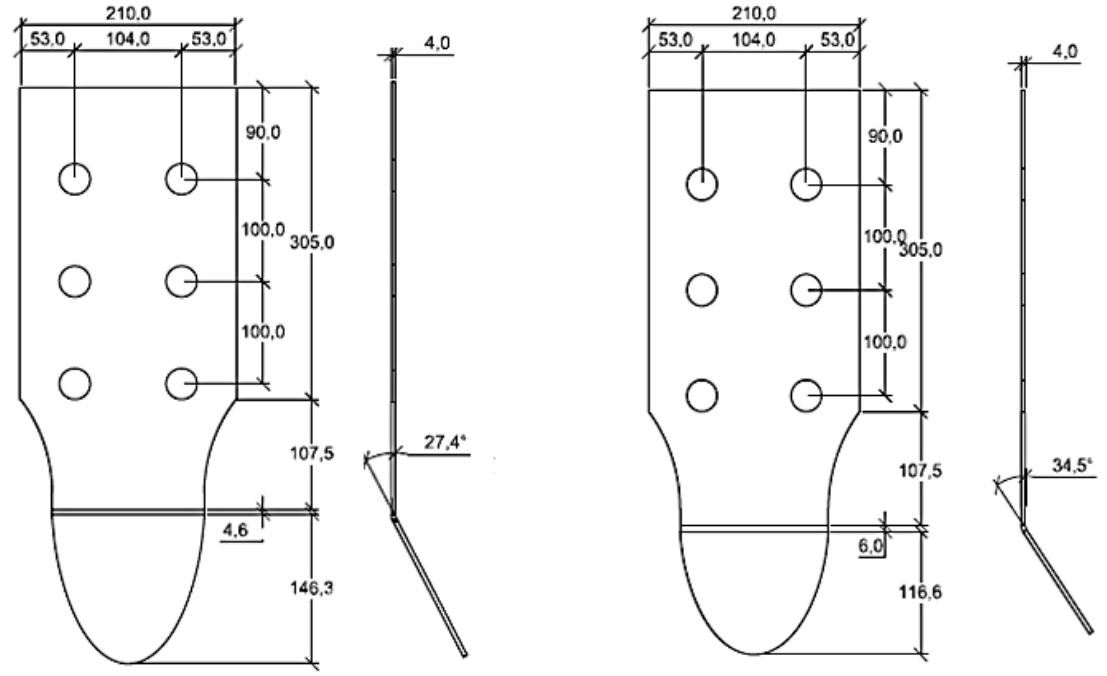


CN 1 CN 3

*Figure 8 Dimensions of the inclined plates with the connecting plate. Units in millimetres.*

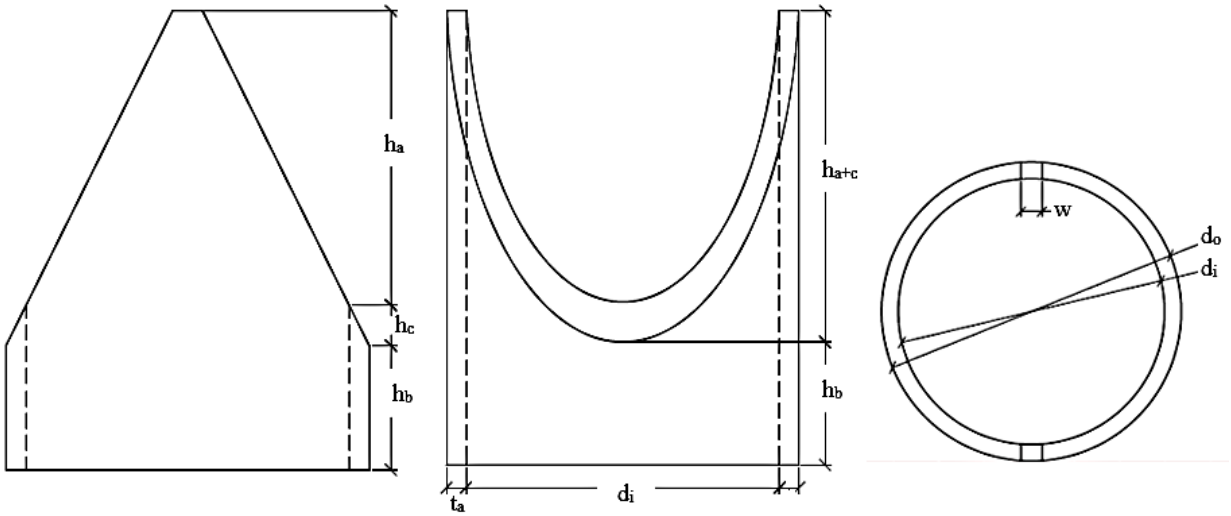


*Figure 9 Dimensions of the CHS for the specmiens.*

The dimensions described in the figure are explained in table 2.

*Table 2 Dimensions on the CHS for the specimens.*

| **Dimension** | **CN 1** | **CN 2** | **CN 3** | **CN 4** |
|---|---|---|---|---|
| **$h_a$ (mm)** | 127.2 | 128.2 | 96.7 | 97.7 |
| **$h_c$ (mm)** | 17.6 | 17.8 | 13.2 | 13.2 |
| **$h_b$ (mm)** | 55.2 | 54.2 | 90.1 | 89.1 |
| **$h_{a+c}$ (mm)** | 144.8 | 145.8 | 109.9 | 124.1 |
| **$t_a$ (mm)** | 8.8 | 8.8 | 8.8 | 8.8 |
| **w (mm)** | 14.2 | 13.2 | 12.5 | 11.2 |
| **$d_i$ (mm)** | 141.4 | 141.4 | 141.4 | 141.4 |
| **$d_o$ (mm)** | 159.0 | 159.0 | 159.0 | 159.0 |

The stiffeners, or the connecting pieces, are of steel grade S355 and fillet welded on place between the two inclined plates, see figure 10. The connecting plate is attached on two of the four specimens, in order to evaluate the effect of its presence. In the connections including the connecting plates, the extruded parts of the inclined plates are widened. The reason of this is that the ultimate load will be higher in these connections due to the load distribution. Since bearing

failure is undesirable in these tests, the plates have to be widened in order to withstand the higher stress.

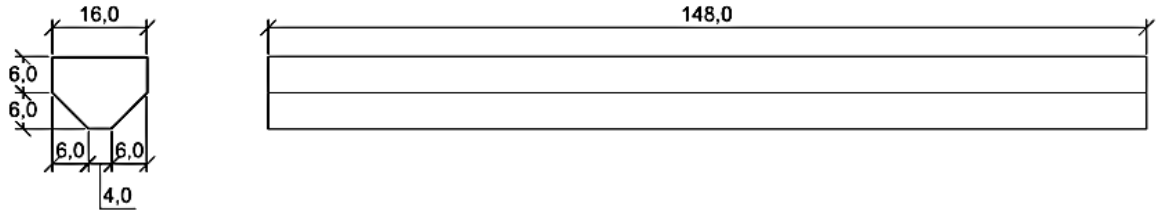


*Figure 10 Dimensions for the connecting plate.*

The connections are designed as a slip-resistant connection and are therefore blasted and painted in accordance with EN 1090-2 class B surface treatment. Faying surfaces are washed with hot steam and shot blasted with G17 grade steel grit. They are then painted with an ethyl silicate zinc rich paint to a thickness of 60 µm.

Between the inclined plates two gusset plates are inserted. The gusset plates are designed with bolt holes in one end and a bigger hole for the pin connection in the other end. In order to distribute the load between the two gussets during the test, a steel ring is inserted in the bigger hole. The gusset plates have two different designs, one for specimen 1 and 3 and one for specimen 5 and 7. These designs are shown in figure 11.

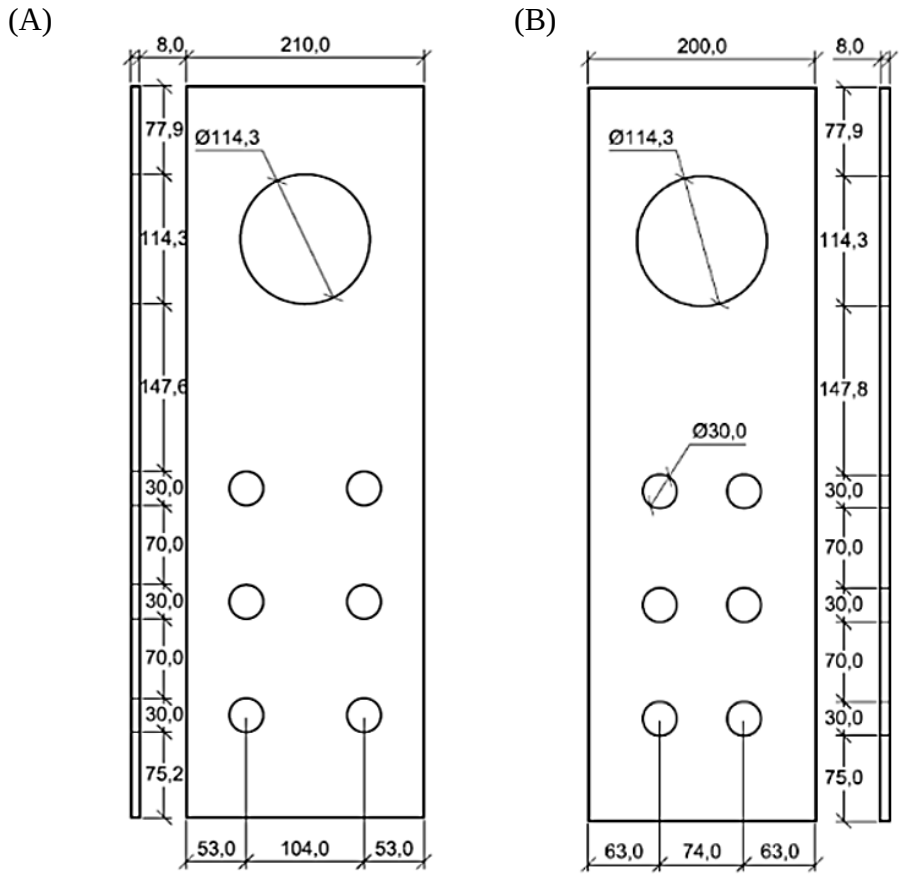


*Figure 11 Dimensions of the gusset plates. (A) is showing the gusset plate for specimen CN 1 and CN 3 while (B) is for specimen CN 2 and CN 4.*

To connect the upper part of the specimens to the test machine a pin is used. The gusset plates are connected between two thicker plates with the pin. These thicker plates are then welded to a bar which is later attached to the test machine. The assembly of the upper part connection is shown in figure 12. The same procedure is done with the lower connection.

*Figure 12 Assembly of the upper connection.*

### 3.3 Bolts

The bolts used in the tests are M27-10.9 hexagonal high strength structural bolts of system HV. Bolts and nuts are both manufactured by FUCHS and meets the demands of EN 14399-4 [24]. Washers are used at the head of the bolts and at the nuts and meets the demand of 14399-1. Dimensions of the bolt system are shown in figure 13.

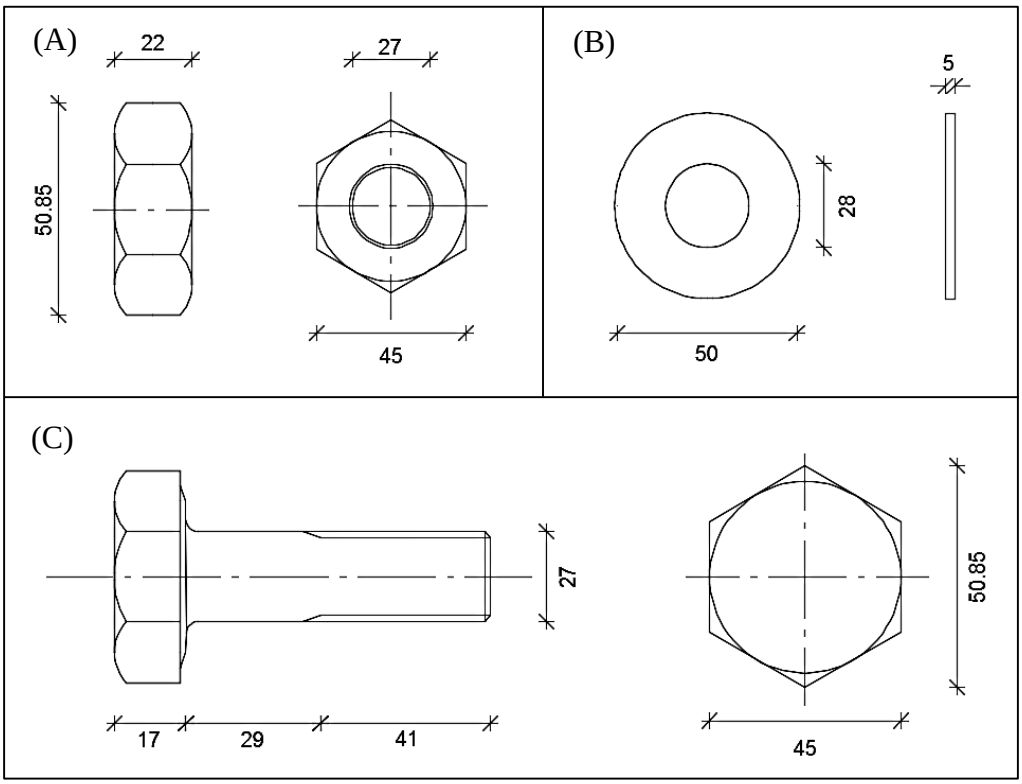


*Figure 13 Dimensions of the bolt set. (A) shows the dimensions of the nut, (B) shows dimenisons of the washer and (C) shows the dimensions of the bolt.*

# 4 HAND CALCULATIONS

*The hand calculation model is based on the plates, bolts and the welds in the specimens. Dimensions on the plates and on the bolts are based on the fixed dimensions of the CHS. The calculations which are performed are slip resistance, bolt pretension and design of the welds. The weld calculations are complex due to the geometry of the semi elliptical weld. All the calculations considers the rules described in the Eurocodes.*

## 4.1 Method

### 4.1.1 Slip resistance

The design slip resistance is calculated according to EN 1993-1-8 section 3.9.1. In this case with the formula

$$F_{s,Rd} = \frac{k_s n \mu}{\gamma_{M3}} F_{p,C} \qquad (4\text{-}1)$$

where

$k_s$ is describing the hole type, given in table 3.

$n$ is the number of friction surfaces

$\mu$ is the slip factor

$F_{p,C}$ is the bolt pre-tension force, see section 4.1.2

*Table 3 Values of $\boldsymbol{k_s}$. Table from EN 1993-1-8* [12].

| Description | $k_s$ |
|---|---|
| Bolts in normal holes | 1.0 |
| Bolts in either oversized holes or short holes with the axis of the slot perpendicular to the direction of load transfer. | 0.85 |
| Bolts in long slotted holes with the axis of the slot perpendicular to the direction of load transfer. | 0.7 |
| Bolts in short slotted holes with the axis of the slot parallel to the direction of load transfer. | 0.76 |
| Bolts in long slotted holes with the axis of the slot parallel to the direction of load transfer. | 0.63 |

### 4.1.2 Pretension of the bolts

The pretension force in the bolts are calculated with the equation

$$F_{p,C} = 0{,}7 f_{ub} A_s \quad (4\text{-}2)$$

where

$f_{ub}$ is the ultimate strength of the bolt

$A_s$ is the tensile stress area of the bolt

In order to obtain the calculated pretension force a moment wrench is used. The wrench registers the torque during the fastening process and therefore the torque that corresponds to the pretension force has to be calculated. The formula used is found in [25] section 8.5.2. According to [24] the bolts have k-class K1 which means that formula 1) must be used.

$$M_{r,1} = k_m d F_{p,C} \quad (4\text{-}3)$$

where

$k_m$ is the friction connection for the bolt

### 4.1.3 Design of welds

In the specimens there are welds that has to be considered. The semi-elliptical weld is the most critical because it attaches the inclined plates with the tube. When calculating these welds the directional method will be used. The equation used in this method is

$$\left[\sigma_\perp^2 + 3\left(\tau_\perp^2 + \tau_\parallel^2\right)\right]^{0.5} \leq \frac{f_u}{\beta_w} \cdot \gamma_M \quad (4\text{-}4)$$

where

$f_u$ is the nominal value of the ultimate strength for the weaker material used.

$\beta_w$ is the correlation factor, and should be taken as 1,0 according to [18]

$\sigma_\perp$ is the normal stress perpendicular to the throat

$\tau_\perp$ is the shear stress, in the plane of the throat, perpendicular to the axis of the weld

$\tau_\parallel$ is the shear stress, in the plane of the throat, parallel to the axis of the weld

In figure 14 a visualisation is shown of the weld together with the stress components explained above.

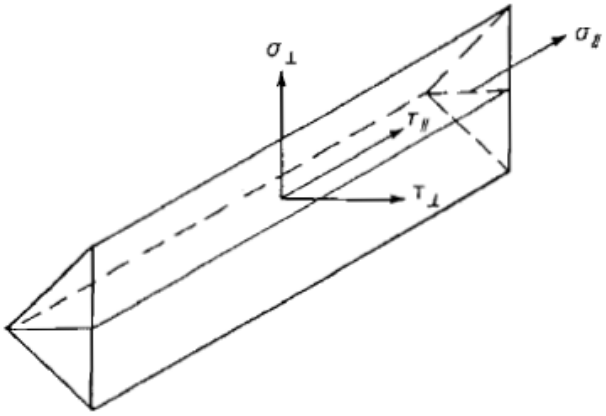


*Figure 14 Stress components for the directional method.* [12]

The stresses are then calculated with equations (4-5) and (4-6) below.

$$\tau_\parallel = \frac{F_y}{A_w} \tag{4-5}$$

$$\sigma_\perp = \tau_\perp = \frac{F_x \cdot sin\theta}{A_w} \tag{4-6}$$

$F_y$ and $F_x$, shown in figure 15, are force components which are calculated from the ultimate load obtained from the FEA.

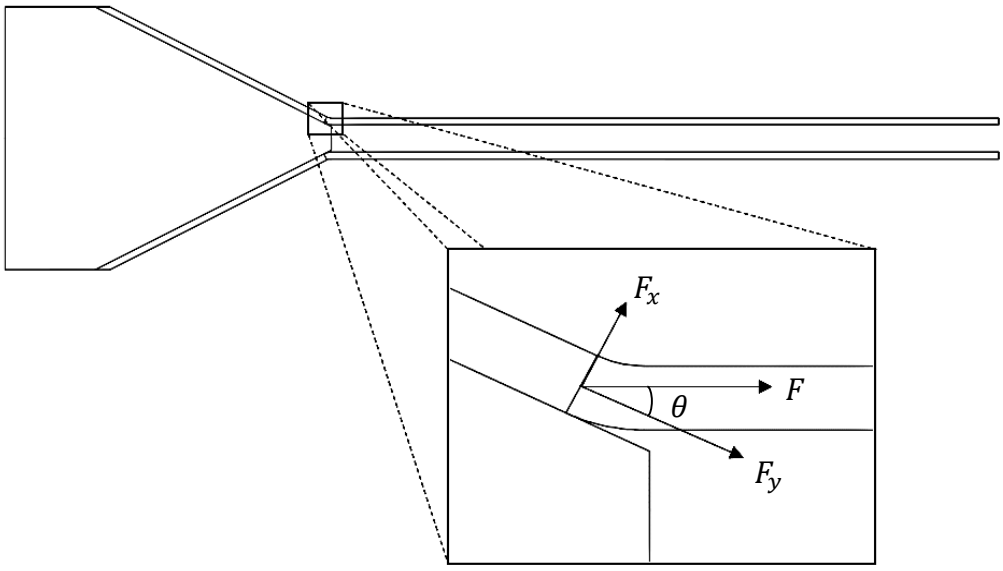


*Figure 15 Enhancement of the force components at the start of the elliptical weld.*

The force components shown in the figure are calculated according to equation 4-7 and 4-8.

$$F_x = F \cdot sin\theta \quad (4\text{-}7)$$

$$F_y = F \cdot cos\theta \quad (4\text{-}8)$$

Before the component forces are calculated, the ultimate load has to be divided by four. The reason for this is that the force will be distributed between the four starting points of the welds. Since the welds are located at the CHS cut, the angle, θ, will be the same as the cut inclination. $A_w$ is the throat area of the weld, which is calculated with

$$A_w = \sum a \cdot l_{act} \quad (4\text{-}9)$$

where

$a$ is the throat thickness explained in section 2.7

$l_{act}$ is the active length of the weld.

The weld geometry for the elliptical weld is not an isosceles triangle which would have created a smaller throat thickness than allowed by the Eurocodes. Since the thickness of the plate is 4 mm the height of the weld cannot be higher than that. The tubes outer diameter is 5.5 mm wider than the plates at both sides. The welds are therefore welded out to the edge, creating a weld foot which is 5.5 mm. The geometry of these welds creates the weld throat showed in figure 16.

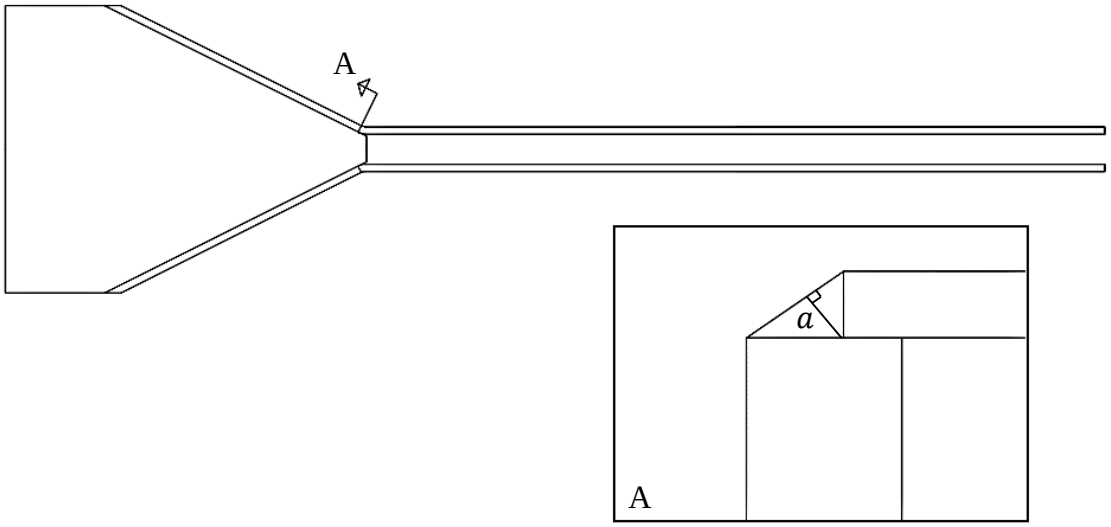


*Figure 16 Illustration of the weld throat dimension for the semi elliptical weld.*

The issue in these calculations is the active length. Due to the complex dimensions of the semi-elliptical weld, the force components changes along the welds length. When calculating the welds only the top part is taken into consideration because it is the straightest part. In the parts where the

weld starts to have a more curved orientation, the properties calculated from the directional method are not valid. A criteria is therefore set in order to decide the outcome of the active length obtained from calculations. If the active length is

$$l_{act} < \frac{1}{2} \cdot l \qquad (4\text{-}10)$$

the approach with the directional method is a good approach. The $l$ in the equation is the length of half the weld. If the active length is longer than this criteria, the approach is not applicable and further research must be carried out. The length which are about to be calculated is further described in figure 17.

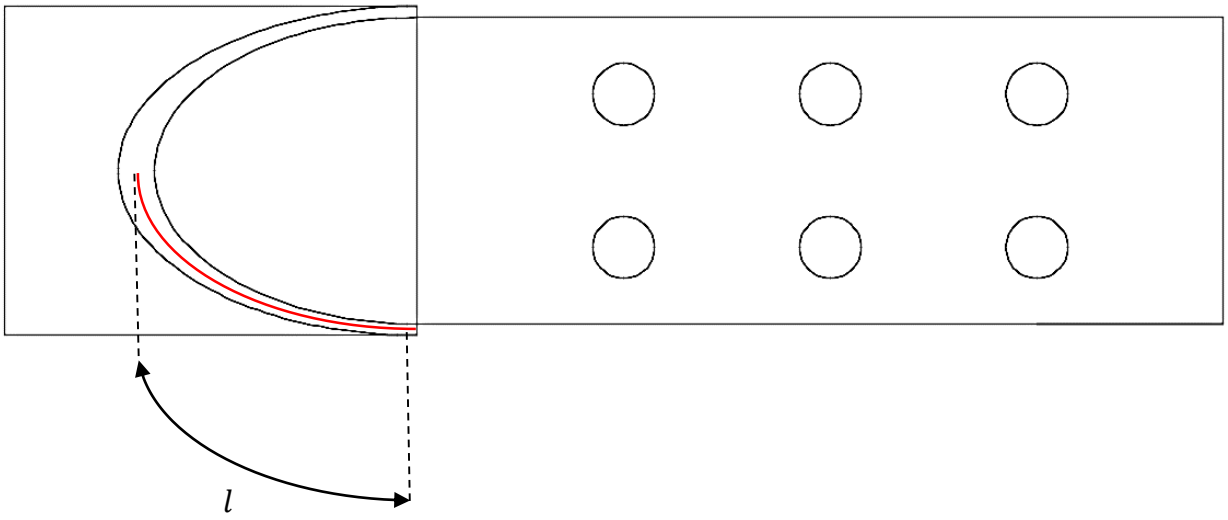


*Figure 17 Illustration of the length, l, which is used in the calculations of the active length.*

With equations (4-4) to (4-9) the formula for active length can be derived as follows. Equation (4-5) and (4-6) in (4-4) gives,

$$\left(\frac{F_x \cdot sin\theta}{A_w}\right)^2 + 3 \cdot \left(\left(\frac{F_x \cdot sin\theta}{A_w}\right)^2 + \left(\frac{F_y}{A_w}\right)^2\right) = \frac{f_u}{\beta_w} \qquad (4\text{-}11)$$

When equation (4-9) is inserted in (4-11) the active length can be derived to the following equation

$$l_{act} = \sqrt{\frac{\left(\left(\frac{F_x \cdot sin\theta}{a}\right)^2 + 3 \cdot \left(\left(\frac{F_x \cdot sin\theta}{a}\right)^2 + \left(\frac{F_y}{a}\right)^2\right)\right)}{\left(\frac{f_u}{\beta_w}\right)^2}} \qquad (4\text{-}12)$$

# 5 FINITE ELEMENT ANALYSIS

*A finite element analysis increases the possibility to more easily investigate details in a test specimen. Parameters like contact pressure and stresses can be hard and sometimes impossible to see in a laboratory test while it is easy to see in a finite element analysis. When the analysis is calibrated with help of a laboratory test it creates the opportunity to make many parametric studies of a specimen. Because of this a lot of time and money can be saved when there is no need to assemble lab specimens. This chapter describes how the tensile test in the previous chapter is analyzed with the help of the finite element method* [22].

## 5.1 Method

### 5.1.1 Model description

The FEA is completed in Abaqus version 6.13. All the specimens is modelled and simulated the same way as the laboratory tests are conducted. All parts have the exact dimensions of the test specimens. The bolts are modeled with a round head instead of a hexagonal head. The reason of this is because it is easier to obtain a good mesh. To create the fine mesh, the bolt has to be properly partitioned. When creating partitions the bolt is divided into several volumes which are appropriate to mesh. The mesh type used is a structure mesh with hexagonal elements. With this mesh type Abaqus creates the mesh on one side of the region and then copies it until the target side is reached [22].

The CHS is also partitioned so that a good mesh can be generated, in this case a structural mesh is obtained. As in the bolts, hexagonal elements are used.

Both the gusset plates and the inclined plates have bolt holes, which creates a distortion in the mesh. In order to solve this, partitions have to be made like in the case with the bolts and the tube. Partitions around the holes are made and the sizes of the mesh elements are adapted to achieve the best results.

### 5.1.2 Material model

In the FEA models two different relationships between stress and strain are considered, nominal and true stress-strain. In annex A, the results from the tensile coupon test are shown in figure 37. The highest value on the yield strength, 792 MPa, and the ultimate strength, 822 MPa, on the tests parallel to the rolling direction is used in the FEA model. The Young's modulus and Poisson's ratio is 210 GPa and 0.3 respectively. These values are known properties for the OPTIM 650 structural steel manufactured by RUUKKI. As mentioned in section 3.2 the steel grade for the tube is S690. In the model the tube is simulated with the same material property as the plates, despite

the different steel grade. The reason of this is that the result is assumed to be unchanged, due to the much thicker cross-section in the tube than in the plates.
In Abaqus the true stress and true plastic strain are used as input to define non-linear material properties. The values received from the tensile coupon tests are nominal stress-strain values and therefore they have to be translated to the true stress-strain values [26]. The equations used to define the true values are,

$$\varepsilon_{true} = \ln(1 + \varepsilon_{nom}) \quad (5\text{-}1)$$

Where

$\varepsilon_{true}$ are the true strains

$\varepsilon_{nom}$ are the nominal strains

The true stress is calculated with the following equation

$$\sigma_{true} = \sigma_{nom}(1 + \varepsilon_{nom}) \quad (5\text{-}2)$$

Where

$\sigma_{true}$ is the true stress

$\sigma_{nom}$ is the nominal stress

The true plastic strain can then be calculated with the results achieved from the equations above. This is done with the equation

$$\varepsilon_{true}^{\text{pl}} = \varepsilon_{true} - \ln\left(1 + \frac{\sigma_{true}}{E}\right) \quad (5\text{-}3)$$

The values from the true stress and the true plastic strain are plotted against each other. In figure 18 the difference between the nominal stress values and the true stress values are shown.

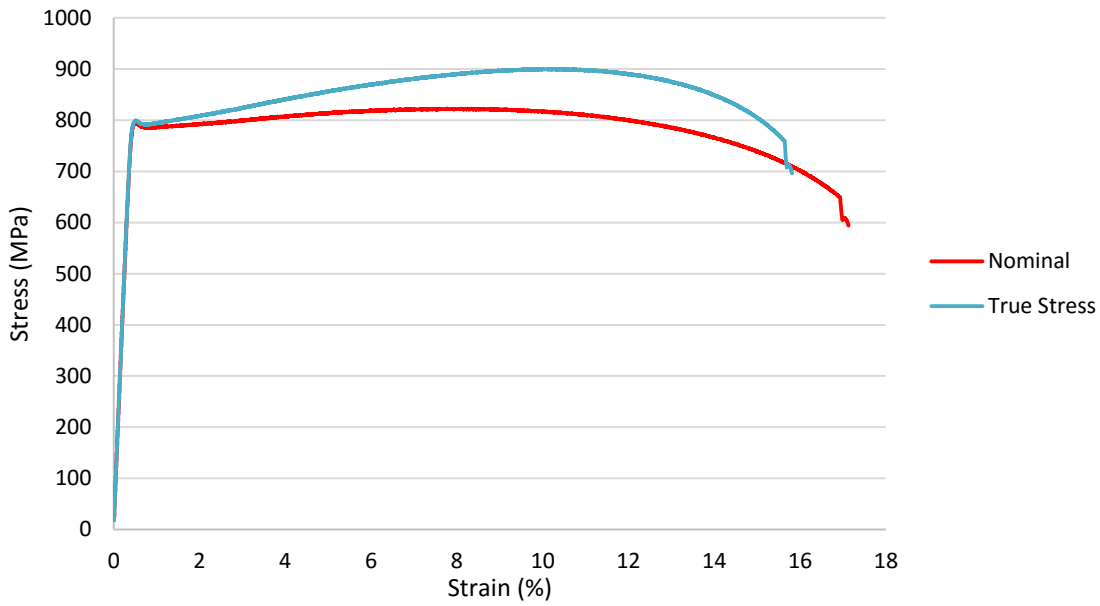


*Figure 18 Nominal and true values of the relationship between stress and strain, steel class S650. Values are taken from tensile test two.*

### 5.1.3 Mesh

The element type used in the model is C3D8R, which is an 8-node brick element. The R at the end of the element name means reduced integration. The reason for choosing that type of element is that it uses a lower order integration to form element stiffness, which reduces the computation time. The size of the element is also an important factor which effects the result of a simulation. A denser mesh creates a more accurate result, but on the other hand gives a longer computation time. In this model two different mesh sizes were used, one denser and one coarser, see figure 19.

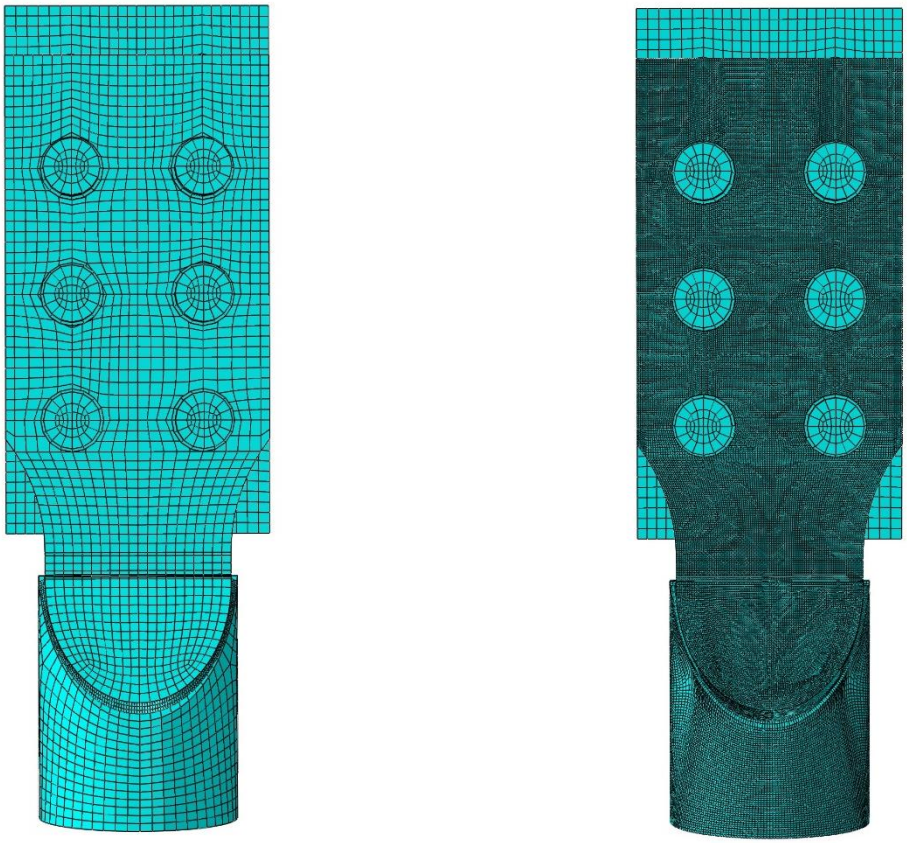

*Figure 19 Specimen CN 3 shown with the two mesh sizes. Coarser mesh to the right and the denser mesh to the left.*

In order to create a model with a more efficient computational time, the parts are meshed with different mesh sizes. The parts where a more accurate result is necessary the mesh is denser. As seen in figure 19 the mesh size is much denser for the inclined plates, the semi-elliptical welds and the CHS. In table 4 the mesh size is presented for the different parts.

*Table 4 Mesh size for the different parts. Value in the parenthesis is for specimen 1 and 3.*

| **Part** | **Mesh size, Dense** | **Mesh size, coarse** |
|---|---|---|
| **Inclined plate** | 1.5 | 8 |
| **Bolt** | 4 | 7 |
| **Gusset plate** | 8 | 8 |
| **CHS** | 2 | 8 |

| | | |
|---|---|---|
| **Connecting plate** | 8 | 8 |
| **Weld** | 1 (0.8) | 2 |

### 5.1.4 Contact interactions

All of the parts in the model are created separately and then assembled. Due to the joints inclination at the end of the CHS, position constraints are used during assembly. This function makes sure that the parts are clamped together without any spacing between them.

In the connection there are different kind of interaction properties. The welds connecting the inclined plates with the CHS, and the weld connecting the connecting plate with the inclined plates are assembled with a tie constraint. The tie formulation chosen for this model is the surface-to-surface. In this formulation one of the surfaces are chosen to be a master surface while the other is chosen as a slave surface. The choice of master and slave surfaces can in some cases have a significant effect on the result. For the best accuracy the slave surface should be chosen as the surface with a finer mesh. The surfaces chosen to be a master or a slave surface are shown in table 5 below.

*Table 5 Chosen master and slave surfaces for the tie-constraints.*

| Pair with TIE-constraint | Master surface | Slave surface |
|---|---|---|
| **Weld-CHS** | Weld | CHS |
| **Weld-Inclined plate** | Inclined plate | Weld |
| **Connecting plate-Inclined plate** | Connecting piece | Inclined plate |

Next step is to simulate contact between plates. Abaqus/Standard provides three different ways for defining contact interactions: general contact, contact pairs, and contact elements. General contact and contact pairs are both surface based contact interactions. Contact elements are used in certain interaction where general contact and contact pairs cannot be modelled. Generally it is recommended to use either general contact or contact pair [26]. The parts which are in contact in the connection are shown in table 6.

*Table 6 Master and slave surface of the parts which are in contact.*

| Parts in contact | Master surface | Slave surface |
|---|---|---|
| **Bolt-Inclined plate** | Bolt | Inclined plate |
| **Inclined plate-gusset plate** | Gusset plate | Inclined plate |
| **Bolt shank-inclined plate** | Bolt | Inclined plate |
| **Bolt shank-gusset plate** | Bolt | Gusset plate |

The interaction properties for the parts in the table 6 was modelled with the contact pairs. With the function "find contact pairs", Abaqus finds all the surfaces which can generate contact.

### 5.1.5 Boundary conditions

Two different kind of steps are used in an Abaqus model, the initial step and the analysis step. The initial step is a step which Abaqus creates at the beginning of a model's step sequence. This step is unique and it cannot be renamed, edited, replaced, copied or deleted. In the initial step, definitions can be made for conditions which are applicable at the beginning of the analysis.

After the initial step follows one or several analysis steps. In each analysis step a specified procedure is defined. For this model two different kinds of analysis steps are created, one for the pre-tensioning of the bolts and one for the connections strength test.

The boundary conditions for the connection are set to be at the top of the gusset plate and at the bottom of the CHS. In order to achieve the best possible result from the model, the boundary conditions has to be defined so that they are similar to those in the lab tests. In the initial step and the pre-tension step, the connection is restrained in all direction, see figure 20.

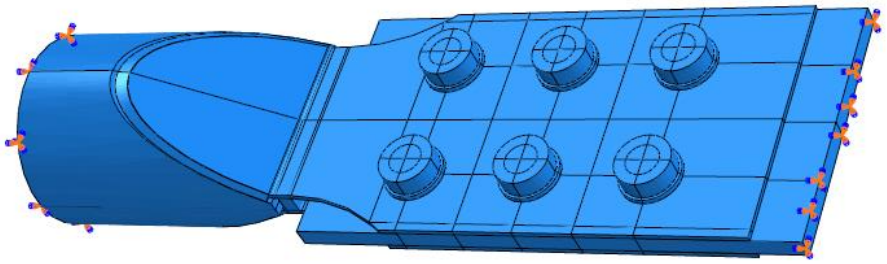

*Figure 20 Specimen CN 1 shown with all DOF restrained at both top and bottom.*

In the last step which simulates the strength test, the boundary conditions are changed. The load is simulated with a displacement assigned at the top of the gusset plate. The restraint at the top of the gusset plate is therefore released in the y-direction, where the displacement is added. The final step can be seen in figure 21.

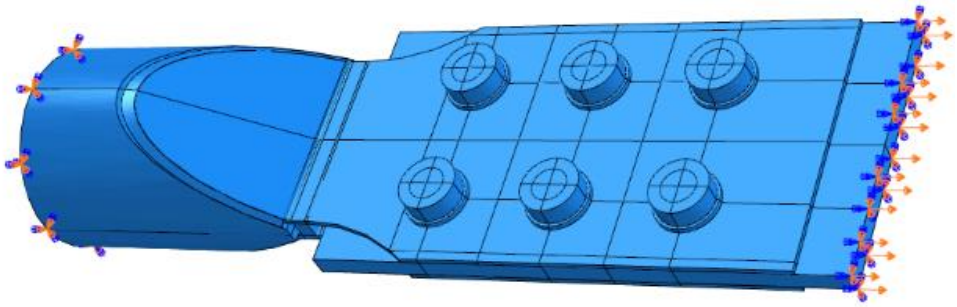

*Figure 21 Specimen CN 1 shown with the predetermined displacement in the y-direction at the top. All DOFs are restrained at the bottom.*

### 5.1.6 Bolt pretension

As in the lab tests the numerical model is simulated with a bolt pretension. To achieve the pretension in the bolt a static, general step is created. In this step a load is created. Since the bolt is a solid region, a datum axis has to be created through the centre of the bolt. This datum axis must also be normal to the cross section of where the load is applied. According to Abaqus documentation, Abaqus offers different ways of applying the bolt load. These are:

- A force is applied to the bolt. When using this method a specified load is applied which creates the pre-tension.

- Bolt length adjustment. This method simulates the tightening by changing the bolts length until it has reached a specific value.

- Bolt is fixed at its current length. This method can only be used after the first analysis step, when a modification is done for a subsequent analysis step. When using this method the bolt length is able to remain constant while the force in the bolt can change according to the response of the model.

In this model the first method is used. The reason of this is that the load applied on the bolt is known. When applying the bolt load a partition has to be made through the centre of the shank of the bolt, see figure 22. The surface in the middle of the shank, created from the partition, and the datum axis are selected when the load is applied [26].

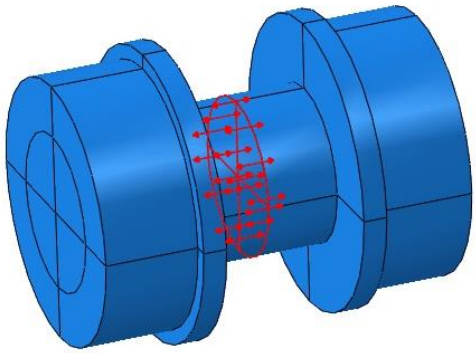

*Figure 22 Bolt pretension created at the midpoint of the shank.*

# 6 EXPERIMENTAL WORK

*The experimental testing consists of four different specimens. All of the specimens are tested until the ultimate strength is reached. Strain gauges are attached on every specimen. The most critical positions to take measurements from are identified with the help of FEA. Results achieved from the experimental tests is later implemented with the FEA, in order to simulate more realistic conditions. The following sections describes the preparation and assembly of the specimens.*

## 6.1 Method

The assembly of the test specimens took place in Complab at Luleå University of technology. The first step in the assembly process was to prepare the specimens for attachment of strain gauges.

### 6.1.1 Strain gauges for tube and plates

The strain gauges used in the tests are produced by Kyowa. Three different sizes were used on the gauges, 1 mm, 2 mm and 5 mm. All of the strain gauges are of model KFG120ΩBiaxial More detailed information about the different gauges are shown in table 7 to 9.

*Table 7 Property description of strain gauge with length 1 mm.*

| Property | Value |
|---|---|
| **Type** | KFG-1-120-D16-11L3M2S |
| **Gauge factor** | 2.04 ± 1.0% |
| **Gauge length** | 1 mm |
| **Gauge resistance** | 119.6 ± 0.4Ω |

*Table 8 Property description of strain gauge with length 2 mm.*

| Property | Value |
|---|---|
| **Type** | KFG-2-120-D16-11L3M2S |
| **Gauge factor** | 2.05 ± 1.0% |
| **Gauge length** | 2 mm |
| **Gauge resistance** | 119.6 ± 0.4Ω |

*Table 9 Property description of strain gauge with length 5 mm.*

| Property | Value |
|---|---|
| **Type** | KFG-5-120-D16-11L3M3S |
| **Gauge factor** | 2.09 ± 1.0% |
| **Gauge length** | 5 mm |
| **Gauge resistance** | 119.6 ± 0.4Ω |

### 6.1.2 Preparation and instrumentation of strain gauges

For the tube and plates all of the gauges are biaxial strain gauges which means that they can measure data in two directions. In total there are 52 strain gauges used for the tube and the plates. A more detailed plan of the quantity and the distribution of the strain gauges can be seen in table 10.

*Table 10 Quantity and distribution of strain gauges.*

| Grid size | Quantity | Per specimen |
|---|---|---|
| **1 mm** | 16 | 4 |
| **2 mm** | 8 | 2 |
| **5 mm** | 28 | 7 |
| **Total** | 52 | 13 |

Strain gauges are placed on both sides of the specimens. The naming of the gauges is sgX, where X is the number of the specific gauge. Since the gauges are biaxial the name is extended with a "v" for vertical data or with an "h" for the horizontal data. The exact positions of the attached gauges can be seen in figure 23. Gauges sg1 and sg2 are placed on the front side adjacent to the weld so that the strain flow can be monitored around that point. Gauges sg3 and sg4 are positioned at the back-side of the specimens in the same positions as sg1 and sg2. Sg5 is positioned at the same height as sg1 but in the middle of the specimens. Sg6 is positioned below sg5, at the tip of the elliptical part. Sg5 and sg6 are positioned at these positions in order to see the behaviour of the plates during loading. Sg7 and sg8 are positioned on the back-side at the same positions as sg5 and sg6 respectively. Sg9 and sg10 are positioned in the middle of the plates to see the bolts effect on

the plates. Sg11 is placed at the end of the plates in order to measure the stresses near the connecting plate. Sg12 and sg13 are placed at the side of the tube in order to see the stress distribution in the tube.

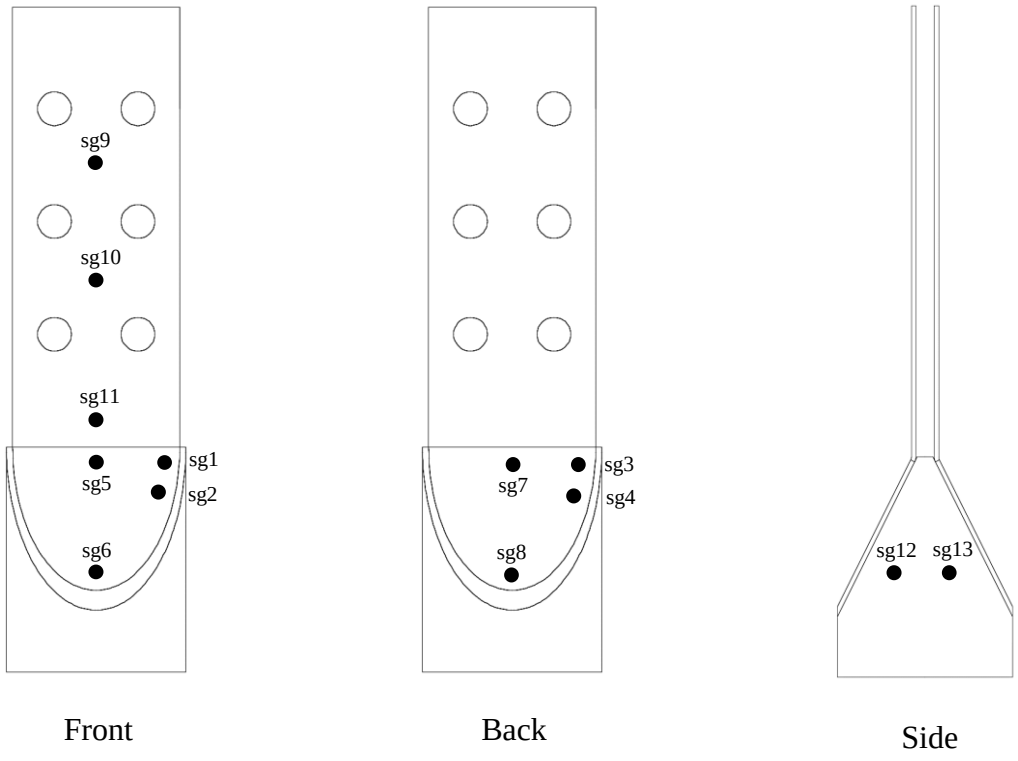


*Figure 23 Positioning of strain gauges. The positions are the same for all specimens. The speccimen in the figure is CN 1.*

The first step in the attachment of the strain gauges was to mark the approximate spots for the gauges. As mentioned in section 3.2 the test specimens were painted, and therefore the paint had to be removed at the specific areas before attaching the strain gauges. The paint at the specific areas was removed by sandblasting.

To achieve the best possible results from the tests, the strain gauges had to be positioned with a certain accuracy. When marking the places for the strain gauges the specimens were hanged with the help of an overhead crane. The specimens were attached in the crane with a pin so that they were able to rotate freely in one direction. With the help of a level an axis could be marked out on three different locations, see figure 24.

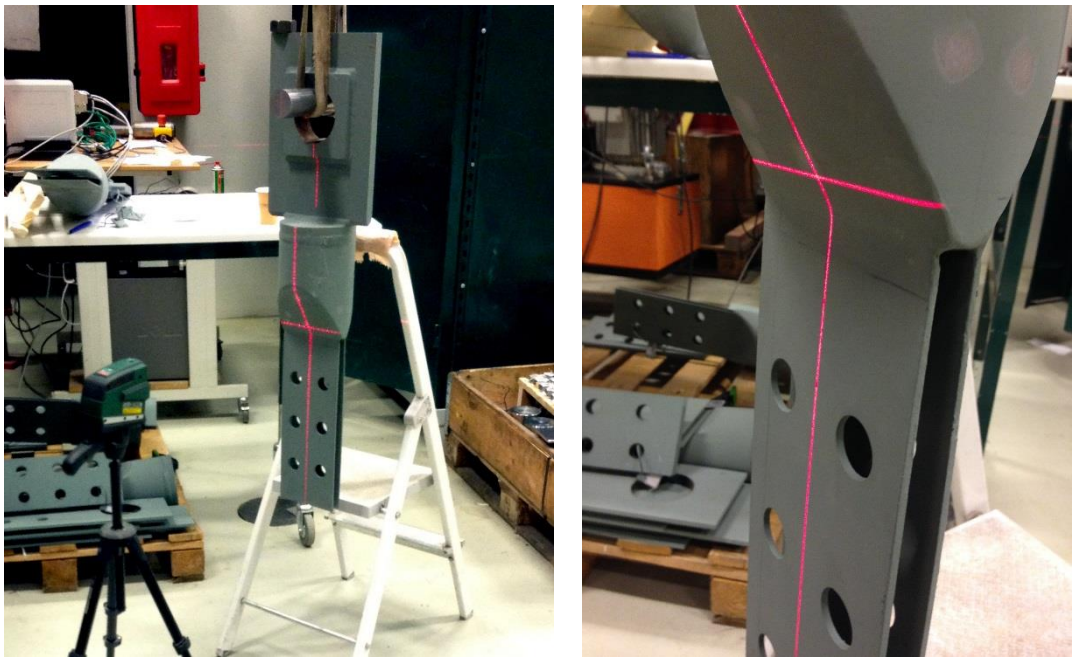

*Figure 24 Marking of axis location.*

When all the spots for the gauges was done two different kind of sandpapers was used to create a clean surface. To get the exact positions for the gauges at the inclined part and at the side of the tube a millimetre paper was attached on those parts. The papers, figure 25, were calibrated from the known axis.

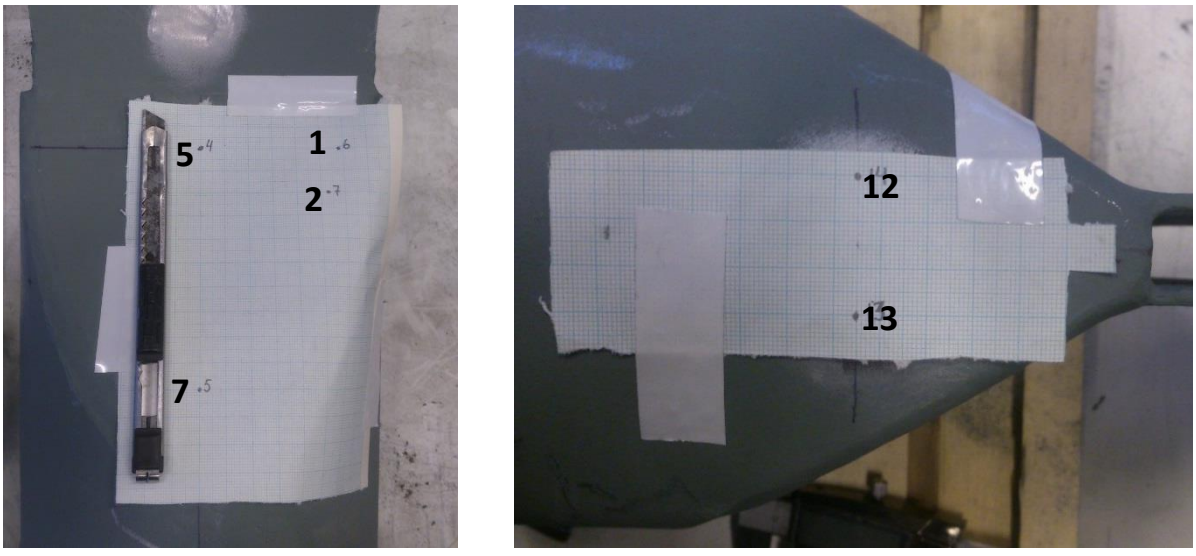


*Figure 25 Strain gauge positioning on the inclined plates and at the side of the tube.*

***Strain gauges for the bolts***

The strain gauges for the bolts are also made by Kyowa. These strain gauges are placed in a 2 mm hole which is drilled through the head of the bolts. The hole is 2 mm in diameter and approximately 30 mm in depth. During the drilling procedure oil is used to cool the drill. When this is done some of the oil is still left inside the hole and can affect the measurements from the strain gauges. In order to remove the oil, the bolts are cleaned with a syringe filled with acetone.
When all the bolts were cleaned they were left over the night to dry. The next step was to glue the strain gauges inside the bolt, figure 26. To get the best result from the strain gauges they are placed 5 mm above the bottom of the hole, according to the instructions from the producer. After the strain gauges were attached properly the bolts were tested in order to calibrate the gauges. More about the calibration can be found in annex B.


*Figure 26 Bolts with strain gauges glued inside the holes.*

***Assembly of test specimens***

The tightening of the bolts were done according to the rules in [25]. The order of the tightening can be seen in figure 27, where bolt 1 is tightened first.

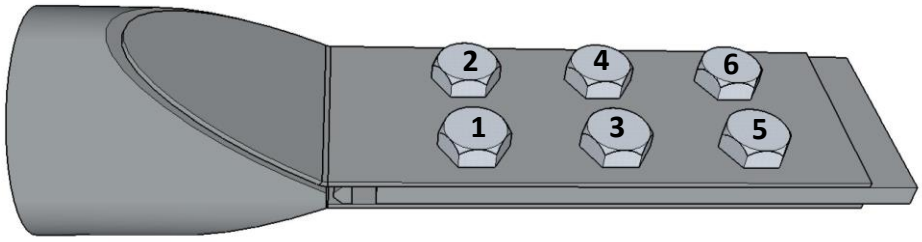


*Figure 27 Tightening order during assembly.*

The tightening procedure was done in several steps, which are summarized in the list below. The reason of the tightening order is that the stiffness is higher near the bevelling angle. Bolt number 1 and 3 has a strain gauge which is monitored during the tightening. In the first step, all the bolts were tightened up to 1800 µm/m or 850 Nm. In the second step the target value was 2420 µm/m. In order to reach that value the bolts were tightened to 2650 m/m before they were released. After releasing the value dropped to the target value, which also is the wanted pretension force. In the list below the tightening is described more carefully in nine steps:

- A torque wrench was calibrated to 850 Nm, for a more accurate tightening. During tightening, the wrench notifies when it reaches the calibrated value.

- The first bolt was tightened with the torque wrench and monitored until it reached 1800 µm/m. When this was done it was discovered that it had to be twisted a more than the wrench notification.

- Bolt number 2 was then tightened. With the results from the first bolt it was tightened with slightly more than the notification from the torque wrench.

- Bolt 3 and 4 are tightened with the same procedure as bolt 1 and 2.

- None of bolt 5 and 6 has an instrumented strain gauge. The tightening is done the same way as for bolt 2 and 4.

- The positioning of the bolts was then marked in order to see the angle they are rotated during the second step.

- Bolt 1 was then tightened up to 2650 μm/m. Bolt 2 was then tightened until it reached the same angle of displacement as bolt 1.

- Bolt 3 and 4 are tightened with the same procedure as bolt 1 and 2.

- Bolt 5 and 6 were then tightened with the same angle of displacement as the two other bolt rows.

# 7 RESULT

## 7.1 Calculation of bolt pretension and slip resistance

### 7.1.1 Pretension of the bolts

The properties needed for the calculation of the pretension force are found in EN 1993-1-8. For bolt size M27 and grade 10.9, the ultimate strength is 1000 MPa and the shear area, $A_s$, is 451 $mm^2$. With the equation from section 4.1.2, the pretension force was calculated to 315.7 kN.

### 7.1.2 Slip resistance

With the calculated value of the pretension force the slip resistance can be calculated. Since all of the bolt holes is normal holes the factor $k_s$ will be 1.0 according to table 12. The number of friction surfaces, n, in the connection is two. The slip factor can be found in table 3.7 in EN 1993-1-8 and is depending on the friction surface class. The surface treatment described in section 3.2 was performed in order to get a surface class B. Equation 4-1 mentioned in section 4.1.1, gave the slip resistance 252.56 kN. In table 11 the calculated values on the slip resistance are shown.

*Table 11 Calculated values on the slip resistance with different slip factor.*

| **Class of friction surface** | **Slip factor, $\mu$** | **Friction surfaces, n** | **$k_s$** | **Slip resistance, $F_{s,Rd}$ (kN)** |
|---|---|---|---|---|
| **A** | 0.5 | 2 | 1.0 | 315.70 |
| **B** | 0.4 | 2 | 1.0 | 252.56 |
| **C** | 0.3 | 2 | 1.0 | 189.42 |
| **D** | 0.2 | 2 | 1.0 | 126.28 |

## 7.2 Finite element analysis

When the FEA is completed, the ultimate load can be reached. The ductility requirements are described in EN 1993-1-3 and EN 1993-1-12 as,

$\varepsilon_u \geq 15\varepsilon_y$

To get a more exact value of this a new criteria is calculated from the values obtained from coupon test two, see figure 28.

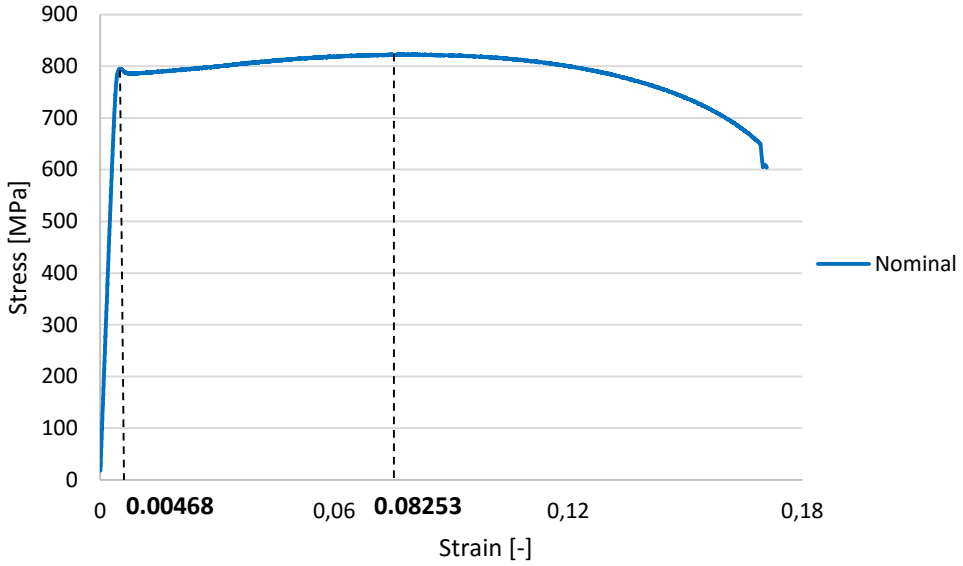


*Figure 28 Strain at the yield stress and at the ultimate stress.*

As the figure shows the strain at yielding, $\varepsilon_y$, is 0.468 % while the ultimate strain, $\varepsilon_u$, is 8.253 %. These values gives the criteria

$$\varepsilon_u \geq 17.69\varepsilon_y$$

When using this limit, the ultimate load will be smaller than if the recommended criteria is used. The load which is considered as the ultimate load is taken from the stage where the material in the connection begins to yield or fulfils the criteria in equation 4-10. When this stage is reached, the achieved loads and displacements are plotted against each other. From this it can be seen at which displacement the ultimate load is reached. As section 6.1.3 described, two different mesh sizes were used. The diagram in figure 29 is showing the obtained curves from Abaqus for both the simulation with the coarser and denser mesh. All the curves ends at 3 mm because of the prescribed displacement explained in section 6.1.5.

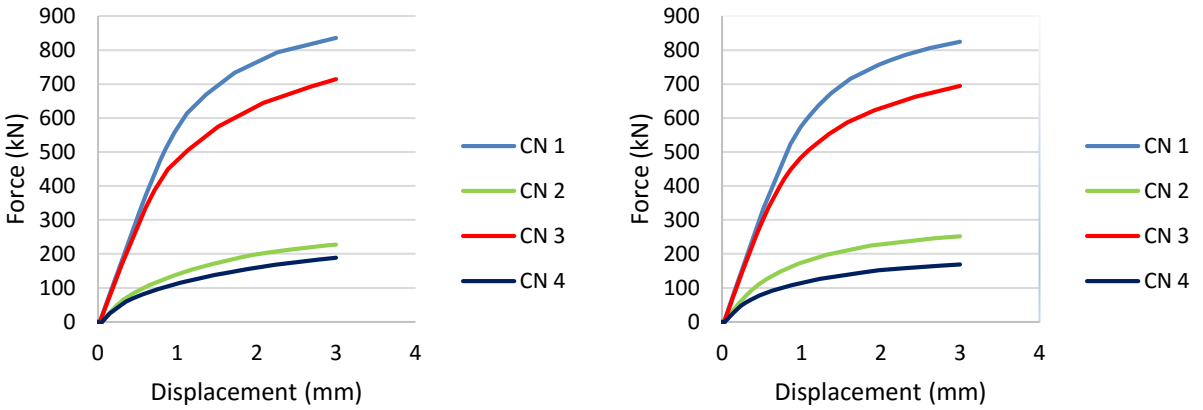


*Figure 29 Force versus displacement diagrams obtained from Abaqus. Results for a coarse mesh (left) and a dense mesh (right).*

The ultimate loads obtained was however recorded before the displacement reached three millimetres. In table 12 the values of the ultimate load are shown for all four specimens with a coarse mesh. The results obtained for the dense mesh are shown in table 13. The results show a large difference between specimens with the connecting plate and without it.

*Table 12 Ultimate load and displacements with coarser mesh.*

| Specimen | Inclination | Connecting plate | Ultimate load (kN) | Displacement at ultimate load (mm) |
|---|---|---|---|---|
| **CN 1** | 1:2 (27.4°) | Yes | 732.7 | 1.722 |
| **CN 2** | 1:2 | No | 142.5 | 1.036 |
| **CN 3** | 1:1.5 (34.5°) | Yes | 505.6 | 1.134 |
| **CN 4** | 1:15 | No | 115.0 | 1.042 |

*Table 13 Ultimate load and displacements with denser mesh.*

| Specimen | Inclination | Connecting plate | Ultimate load (kN) | Displacement at ultimate load (mm) |
|---|---|---|---|---|
| **CN 1** | 1:2 | Yes | 672.6 | 0.216 |
| **CN 2** | 1:2 | No | 147.1 | 1.375 |
| **CN 3** | 1:1.5 | Yes | 481.1 | 0.985 |
| **CN 4** | 1:1.5 | No | 107.9 | 0.873 |

As it can be seen in the table the ultimate load is decreasing when a denser mesh is used. Because the denser mesh gives more accurate result these values will be used in future calculations.

## 7.3 Experimental work

The experimental tests were performed with a displacement control of 0.05 mm/sec. In figure 30 the load versus displacement curves obtained from the tests are shown.

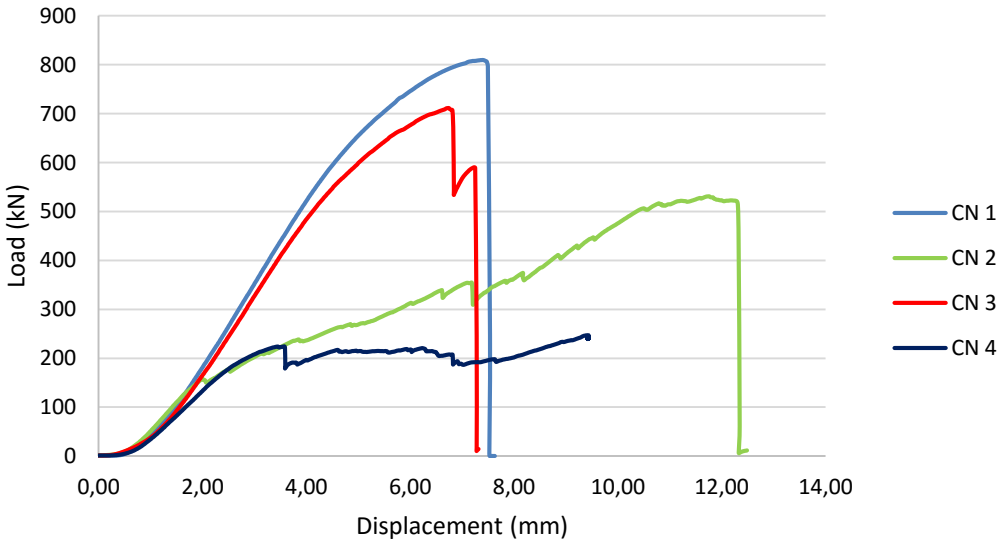


*Figure 30 Load versus displacement curves from the experimental work for each specimen.*

As the diagram shows, the load for the stiffened specimens are increasing until it reaches the ultimate load, 809.9 kN for CN 1 and 711.8 kN for CN 3, where it instantly fails. The ultimate load and the corresponding displacement are shown for each specimen in table 15 below.

*Table 14 Ultimate load and displacements from the experimental work.*

| Specimen | Inclination | Connecting piece | Ultimate load (kN) | Displacement at ultimate load (mm) |
|---|---|---|---|---|
| **CN 1** | 1:2 | Yes | 809.9 | 7.40 |
| **CN 2** | 1:2 | No | 521.7 | 11.2 |
| **CN 3** | 1:1.5 | Yes | 711.8 | 6.74 |
| **CN 4** | 1:1.5 | No | 247.2 | 9.43 |

## 7.4 Calculation of semi-elliptical welds

### 7.4.1 Weld calculations with results from FEA

The known properties for the calculations are presented in table 16 below. The values on the force are from the FEA with a higher mesh density.

*Table 15 Known properties for the test specimens. The force, F, is achieved from experimental tests.*

| Specimen | $f_u$ [MPa] | $\beta_w$ [-] | $F$ [kN] | $a$ [mm] |
|---|---|---|---|---|
| **CN 1** | | | 672.6 | |
| **CN 2** | 822.4 | 1.0 | 147.1 | 3.235 |
| **CN 3** | | | 481.1 | |
| **CN 4** | | | 107.9 | |

In table 17 the calculated force components and the active lengths are presented for the specimens with the higher mesh density.

*Table 16 Calculated values for the force components and the effective length.*

| Specimen | $F_x$ [kN] | $F_y$ [kN] | $l_{act}$ [mm] |
|---|---|---|---|
| **CN 1** | 74.04 | 151.0 | 101.3 |
| **CN 2** | 16.20 | 33.03 | 22.16 |
| **CN 3** | 66.92 | 99.93 | 70.83 |
| **CN 4** | 15.01 | 22.42 | 15.89 |

### 7.4.2 Weld calculations with results experimental tests

The known properties for the calculations are presented in table 18 below. The values on the force are from the experimental tests.

*Table 17 Known properties for the test specimens. The force, F, is achieved from FEA.*

| Specimen | $f_u$ [MPa] | $\beta_w$ [-] | $F$ [kN] | $a$ [mm] |
|---|---|---|---|---|
| **CN 1** | | | 809.9 | |
| **CN 2** | 822.4 | 1.0 | 158.0 | 3.235 |
| **CN 3** | | | 711.8 | |
| **CN 4** | | | 223.9 | |

In table 19 the calculated force components and the active lengths are presented for all of the tested specimens.

*Table 18 Calculated values for the force components and the effective length.*

| Specimen | $F_x$ [kN] | $F_y$ [kN] | $l_{act}$ [mm] |
|---|---|---|---|
| **CN 1** | 89.16 | 181.8 | 122.0 |
| **CN 2** | 17.40 | 35.47 | 23.80 |
| **CN 3** | 99.01 | 147.9 | 104.8 |
| **CN 4** | 31.15 | 46.51 | 32.97 |

# 8 ANALYSIS

## 8.1 Hand calculations

### 8.1.1 Weld calculations with results from FEA

The criteria that was set in equation (4-10), to determine if the calculation method used was the right approach, is now considered. The check if the criteria is fulfilled can be seen in table 20.

*Table 19 Criteria check of the active length using results from FEA.*

| **Specimen** | **Active length, $l_{act}$ [mm]** | **Assumption, $\frac{l}{2}$ [mm]** | **Assumption check, OK if $l_{act} < \frac{l}{2}$** | **Percentage of length, $l_{act}$ [%]** |
|---|---|---|---|---|
| **CN 1** | 6.772 | 83.954 | NOT OK | Exceeding 100 % |
| **CN 2** | 40.803 | 83.954 | OK | 49 |
| **CN 3** | 5.703 | 72.350 | OK | 8 |
| **CN 4** | 30.123 | 72.350 | OK | 41 |

As it can be seen in table 20 the active length is longer than the assumed length in specimen CN 1. Due to the higher ultimate load obtained for this specimen, more of the weld has to be activated to withstand the load. Specimen CN 3 is not exceeding the assumed length, thus the ultimate load is lower than for specimen CN 1. For specimen CN 2 and CN 4 the active length is shorter than the assumption. Due to the lack of the connecting piece in these specimens the stresses are concentrated near the welds. The inclined plates straightened with increased load which meant that the welds was progressively ripped off.

### 8.1.2 Weld calculations with results from experimental tests

The active lengths obtained using the result from the experimental tests are longer than for the FEA. In table 21, the assumption check is shown for all specimens.

*Table 20 Criteria check of the active length using results from experimental tests.*

| **Specimen** | **Active length, $l_{act}$ [mm]** | **Assumption, $\frac{l}{2}$ [mm]** | **Assumption check, OK if $l_{act} < \frac{l}{2}$** | **Percentage of length, $l_{act}$ [%]** |
|---|---|---|---|---|
| **CN 1** | 6.772 | 83.954 | NOT OK | Exceeding 100 % |
| **CN 2** | 40.803 | 83.954 | OK | 49 |
| **CN 3** | 5.703 | 72.350 | NOT OK | Exceeding 100 % |
| **CN 4** | 30.123 | 72.350 | OK | 42 |

As the table is showing the assumption is not good for specimen CN 1 and CN 3. The ultimate load obtained from the experimental tests was higher than from the FEA, which lead to longer active lengths in all of the specimens. Due to this, the active length exceeded the assumed length for both specimen CN 1 and CN 3.

## 8.2 Experimental work

As it was shown in section 7.3 the curves were much more continuous for specimens CN 1 and CN 3 than for specimen CN 2 and CN 4. The shape of the curves can be explained with different failure patterns for the specimens. Specimen CN 1 and CN 3, which are shown in figure 31, clearly shows a higher ultimate load than CN 2 and CN 4. These connections is however showing a much more brittle failure.

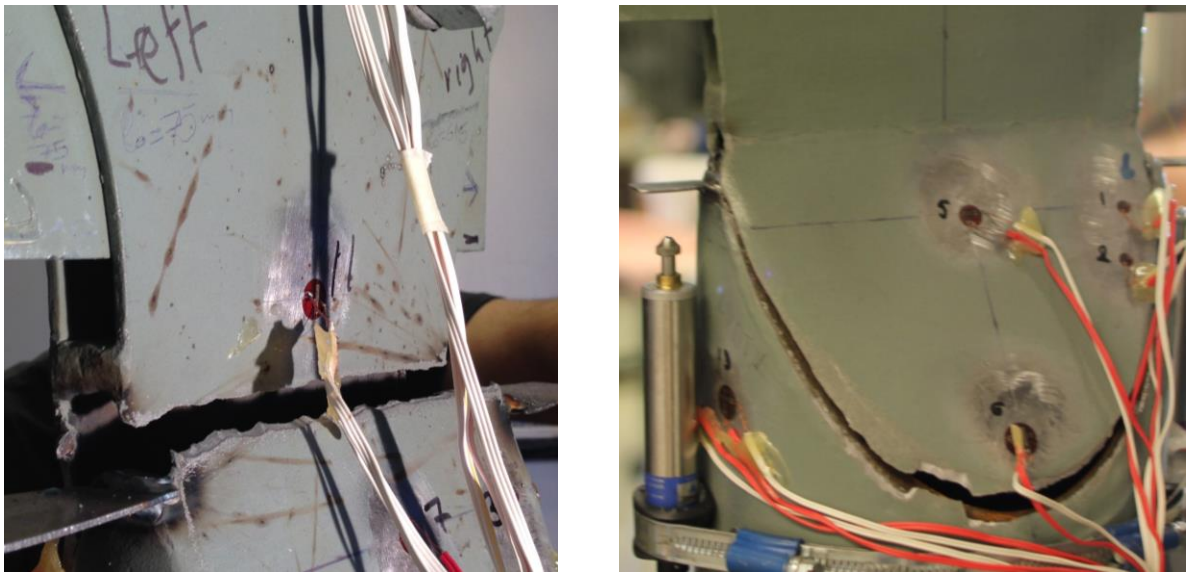


*Figure 31 Fracture for specimen CN 1, right, and CN 3, left.*

For CN 1 the stiffener in combination with good weldment ruptured the inclined plate at its bended part. For CN 3 the whole weld fractured and was detached from the CHS. However, good weldment resulted in weld fracture along the shear plane. CN 2 and CN 4, shown in figure 32, showed a more progressive failure. These specimens' started to fail at 160 kN and 220 kN respectively, nevertheless the resistance for the specimens still increased. For CN 2 the resistance increased up to 510 kN before it decreases and reaches a total failure. CN 4 was not tested up to total failure due to the limited stroke of the testing equipment. The maximum resistance recorded during the tests was 230 kN.

*Figure 32 Fracture for specimen CN 1, right, and CN 3, left.*

For both specimen CN 2 and CN 4 the fracture propagated along the weld, starting at the weld tip. Due to the lack of a connecting piece in these specimens, the deflection of the inclined plates near the CHS fractured the weld. When more load was applied the lower parts of the welds started to activate as the inclined plates straightened. The ultimate loads obtained from the tests are compared both with the respect of the connecting piece and bevelling angle. In table 22 the load increase due to the connecting piece is shown.

*Table 21 Load increase due to the presence of the connecting piece.*

| Specimen | Inclination | Connecting piece | Ultimate load (kN) | Load increase with connecting piece (%) |
|---|---|---|---|---|
| **CN 1** | 1:2 | Yes | 809.9 | 55 |
| **CN 2** | 1:2 | No | 521.7 | |
| **CN 3** | 1:1.5 | Yes | 711.8 | 188 |
| **CN 4** | 1:1.5 | No | 247.2 | |

When a comparison is made between the specimens with and without the connecting piece a big difference in ultimate load can be seen. When comparing specimens CN 1 and CN 2 the ultimate load increases with 55 %. When comparing specimens CN 3 and CN 4 the ultimate load can be increased up to 188 %, then again specimen CN 4 was not tested until total failure. If this test would have continued, the ultimate load might have been higher than the present results shows. The comparison between specimen CN 1 and CN 2 can therefore be seen as more trustworthy. In the experimental work it was also shown that the specimens with inclination 1:2 have a slightly higher ultimate load than the specimens with inclination 1:1.5. The increase in ultimate load is shown in table 23.

*Table 22 Load change due to smaller bevelling angle.*

| Specimen | Inclination | Connecting piece | Ultimate load (kN) | Load increase with smaller bevelling angle piece (%) |
|---|---|---|---|---|
| **CN 1** | 1:2 | Yes | 809.9 | 14 |
| **CN 3** | 1:1.5 | Yes | 711.8 | |
| **CN 2** | 1:2 | No | 521.7 | 111 |
| **CN 4** | 1:1.5 | No | 247.2 | |

As the table shows, the increase of ultimate load is around 14 % between specimen CN 1 and CN 3 while it is 111 % between CN 2 and CN 4. The increase between CN 1 and CN 3, is for the same reason as with the connecting piece, seen as the more trustworthy result.
If the comparison is made when the specimens started to fractured, the results can be more reliable when comparing CN 2 and CN 4. Fracture for specimen CN 1 and CN 3 is the same as the load for total failure. For specimens CN 2 and CN 4 fracture occurs at 158.0 kN and 223.9 kN respectively. In tables 24 and 25 the load increase is shown.

*Table 23 Load change due to the presence of the connecting piece.*

| Specimen | Inclination | Connecting piece | Ultimate load (kN) | Load increase with connecting piece (%) |
|---|---|---|---|---|
| **CN 1** | 1:2 | Yes | 809.9 | 413 |
| **CN 2** | 1:2 | No | 158.0 | |
| **CN 3** | 1:1.5 | Yes | 711.8 | 218 |
| **CN 4** | 1:1.5 | No | 223.9 | |

*Table 24 Load change due to a smaller bevelling angle.*

| Specimen | Inclination | Connecting piece | Ultimate load (kN) | Load change with smaller bevelling angle (%) |
|---|---|---|---|---|
| **CN 2** | 1:2 | No | 158.0 | -29 |
| **CN 4** | 1:1.5 | No | 223.9 | |

As it can be seen in the table 25 the load is decreasing with a smaller bevelling angle.

### 8.2.1 Stress and strain distribution

The strain gauges attached on the specimen measures data at the positions where stress distribution is most interesting. As it was explained in the previous section, the specimens fractured along the weld or near the weld. Due to this, the strain gauges near these positions are investigated. In figure 33 the strain at gauge position sg1v and sg3v is plotted with the respect of time. The figure only considers the strain in specimen 1 and 3.

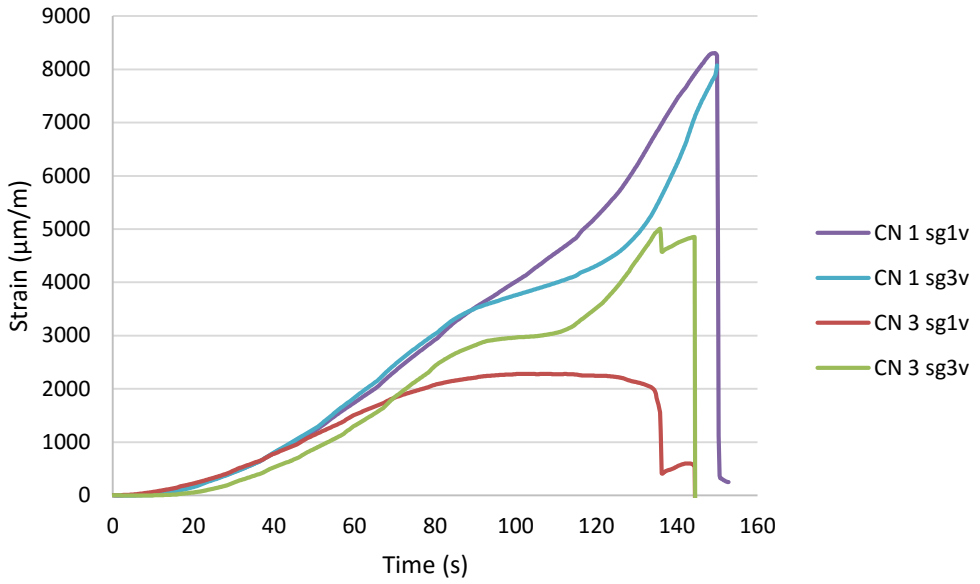


*Figure 33 Diagram showing the strain with the respect of time at gauge position sg1v and sg3v for specimen CN 1 and 3.*

As it was mentioned in section 8.2, the connections ultimate load increased with a smaller bevelling angle. The diagram in figure 33 also proves this statement, due to a higher strain in specimen CN 1 compared to specimen CN 3. Specimen CN 1 reached a maximum strain of 8267 µm/m before the strain gauges broke. Specimen CN 3 only reached 4851 µm/m before it suffered excessive damage. Strain gauges sg2v and sg4v which is attached under sg1v and sg3v are shown in figure 34.

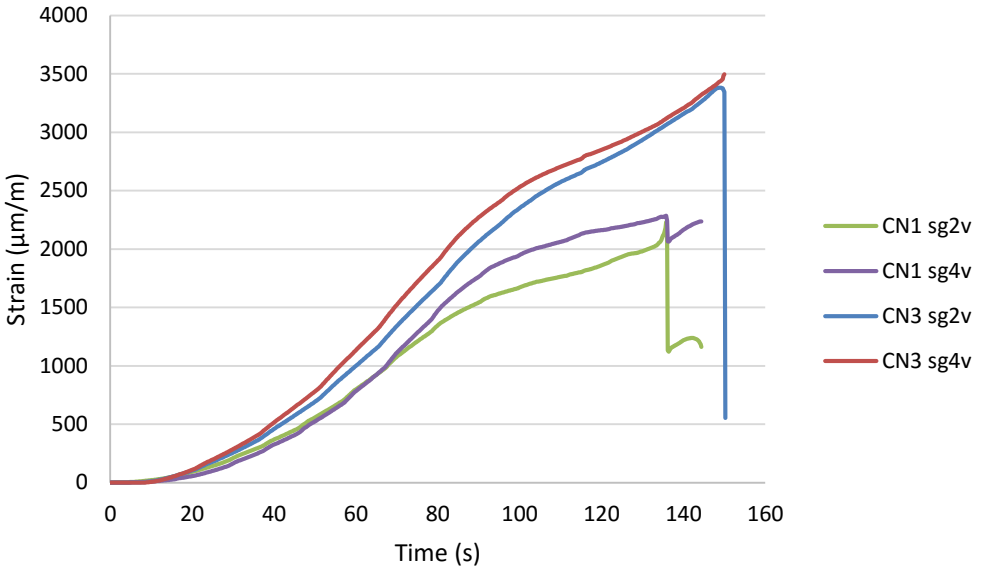


*Figure 34 Diagram showing the strain with the respect of time at gauge position sg2v and sg4v for specimen CN 1 and 3.*

The diagram shows as in the previous figure that the strain is much higher for the specimen's with a smaller bevelling angle. At this position the strain does not reach the yield limit for the steel since the strain is much lower than at gauge position sg1v and sg3v. The strain for specimen CN 1 reached a maximum of 3409 µm/m while it reached 2285 µm/m for specimen CN 3. The values obtained from specimen CN 2 and CN 4 are not analysed here due to the specimen's progressive failure. The strain seen in the diagrams is varying in such a way that the result can be seen as inaccurate.

### 8.2.2 Slip resistance

The connections are designed in such a way that any slip should not occur. The results from the experimental test showed that the calculations of the slip resistance was accurate. The lvdt's used during the tests did not record any slip. If there would be any slip, the curves would have make a rapid increase in displacement. The bolt holes are three millimetres larger than the bolts, which means that there is a 1.5 millimetre space between the plate and the bolt. If a slip occurred it should be around this value, assumed that the connection is assembled correctly. A slip of that magnitude was not recorded during the tests.

### 8.2.3 Behaviour of the tube

The behaviour of the tube is also important to consider. As it was shown in figure 23, strain gauges were attached at the side of the tube. The results from these showed that all CHS's in the experiment deformed elastically. In figure 35 the maximum strain from strain gauges sg12v and sg13v are shown for all of the specimens.

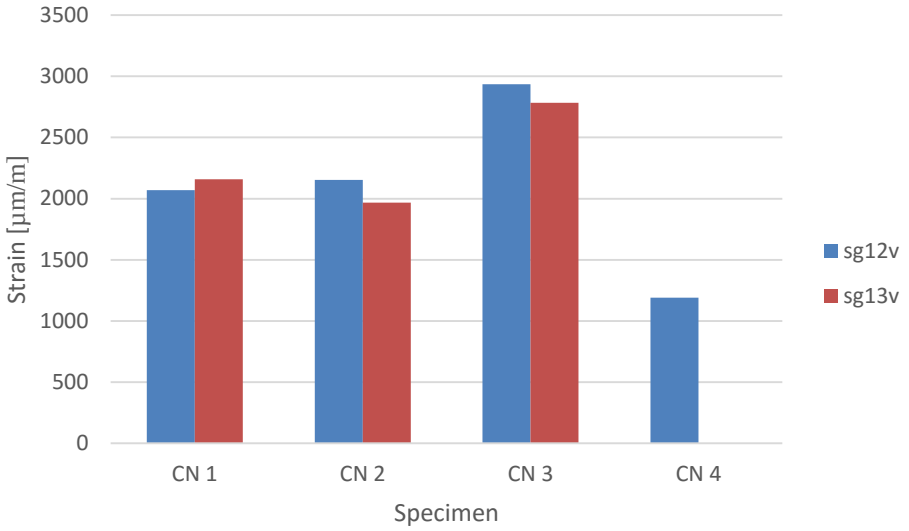


*Figure 35 Strain versus time for strain gauges sg12v and sg13v at specimen CN 1 and CN 3.*

For specimen CN 1 and CN 3 almost a linear increase is recorded, until it reaches 2936 µm/m for CN 3 and 2157 µm/m for CN 1. The increase is very similar to the load versus displacement curves in figure 30. The highest strain obtained for specimen CN 2 and CN 4 is shown in figure 35. The bars shown in the figure is not showing any result from strain gauge sg13v on specimen CN 4. The reason of this is that the gauge was detached during loading. The increase for CN 2 and CN 4 is not similar to the increase explained for CN 1 and CN 3. The progressive failure of the connection is making the tube to first have a strain increase followed by a strain decrease. Specimen CN 2 reaches a strain of 2154 µm/m before it starts to decrease while specimen CN 4 reaches 1192 µm/m before decreasing. The reason of the decrease is due to the failure of the weld. When the inclined plates started to detach from the CHS, the stresses redistributed. When the fracture of the weld started progressing, the stresses started to decrease at the gauge positions.

When comparing the different specimens it can be seen that the strain became much higher for the specimens with the connecting piece. With the inclination 1:2 the strain is 0.1 % higher for specimen CN 1 than for specimen CN 2. For the specimens with the inclination 1:1.5 the strain is 146 % higher for specimen CN 3 than for specimen CN 4. When comparing the two different inclinations two different cases are seen. The specimens with the connecting piece, specimen CN 1 and CN 3, are showing 36 % higher strain for the larger inclination. For specimen CN 2 and CN 4 the strain is 81 % higher with the smaller inclination. As mentioned in section 8.2, specimen CN 4 was not tested up to total failure, which makes it hard to compare the specimen with the other specimens.

## 8.3 Finite element analysis

### 8.3.1 Ultimate load

All the ultimate loads are obtained when the weld begins to fail. Because of the triangular shape of the welds the brick elements are distorted, especially at the beginning of the weld. Due to this a cross section is made at a small distance from the weld start. At this position the stresses and strains are seen as more realistic, and therefore obtained from this point. The result clearly showed the difference between the specimens with and without the connecting piece. The ultimate load became much higher when the connecting piece was present. In table 26 below, the ratio between with and without the connecting piece is shown.

*Table 25 Ratio between with and without the connecting piece.*

| Specimen | Inclination | Connecting piece | Ultimate load (kN) | Load increase with connecting piece (%) |
|---|---|---|---|---|
| **CN 1** | 1:2 | Yes | 672.6 | 357 |
| **CN 2** | 1:2 | No | 147.1 | |
| **CN 3** | 1:1.5 | Yes | 481.1 | 346 |
| **CN 4** | 1:1.5 | No | 107.9 | |

A difference was also seen with different bevelling angle. If the bevelling angle was bigger the ultimate load decreased. In table 27, the ratio between the different bevelling angles is shown.

*Table 26 Ratio between the different bevelling angles.*

| Specimen | Inclination | Connecting piece | Ultimate load (kN) | Load increase with smaller bevelling angle (%) |
|---|---|---|---|---|
| **CN 1** | 1:2 | Yes | 672.6 | 40 |
| **CN 3** | 1:1.5 | Yes | 481.1 | |
| **CN 2** | 1:2 | No | 147.1 | 36 |
| **CN 4** | 1:1.5 | No | 107.9 | |

### 8.3.2 Stress and strain distribution

From the finite element analysis it can be seen that all of the specimens started to fail at the start of the elliptical weld. The weld failed at the weld root and was then spread through the length of the weld. For specimen CN 1 and CN 3 high stresses were seen at the bending of the inclined plate. This stress distribution was distributed rapidly over the width of the plates when more displacement was introduced.

The step in the model which was the most observed was the last step in the analysis, where the tension was introduced. When the stress distribution was analysed it could be seen that the stresses increased at an early stage in the simulation. All of these early stage stresses were focused in the area around the elliptical weld and the bended part of the inclined plate.

## 8.4 Comparison between experimental work and FEA

When comparing the experimental results with the results from the FEA it was noticed that the ultimate load was higher in the experimental tests, figure 36. The ultimate load that were used in the comparison was the highest load before any load reduction. This meant that the ultimate loads, from the experimental tests, used for specimen CN 2 and CN 4 were 158.0 kN and 223.9 kN respectively.

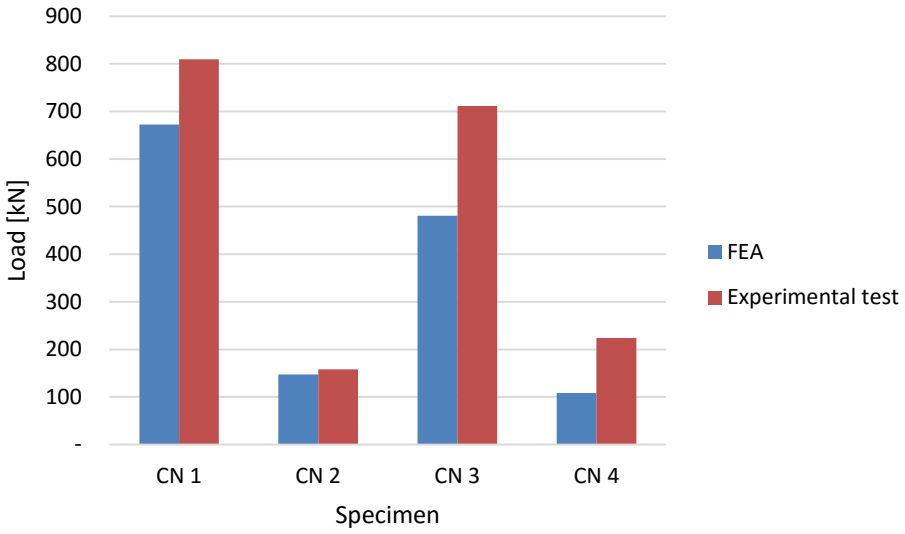


*Figure 36 Comparison of the ultimate load between the FEA and the experimental test.*

As seen in the figure the ultimate load was higher in the experimental tests than in the FEA. For the specimens CN 1 and CN 3 the ultimate load was 20 % and 50 % larger in the experimental tests. For specimens CN 2 and CN 4 the ultimate load was 7 % and 107 % larger. The deviation was especially large for specimen CN 3 and CN 4, which were the specimens with the larger bevelling angle.

When a comparison between the displacements were made it could be seen that the specimens from the experimental tests had a bigger displacement. In the FEA the displacement introduced was 3 millimetres, but the specimens reached the ultimate load before this value. One explanation for this is the mounting pieces used in the experimental tests. As mentioned in section 6.1.5, the FEA models were fixed in all directions at the bottom of the CHS while the displacement was introduced on the gusset plate. In the experimental tests the mounting pieces deformed elastically and creates a displacement not considered in the FEA.

The CHS does not suffer any critical stress values in neither the FEA nor the experimental tests. As seen in 8.2.3 the CHS's did not reach the yield limit. In annex C, figure 41 to figure 48, only lower stress values can be seen in the CHS's.

# 9 DISCUSSION

## 9.1 Hand calculations

In the hand calculation model, the calculations made for the semi elliptical weld is seen as an uncertainty. The reason is because of the curvature of the weld and the inclination of the CHS cut. In order to achieve a good calculation model for the weld more research has to be done to create a proper approach. Another thing that has to be investigated further is the thickness of the CHS. If the thickness of the CHS is decreased, the thickness of the plates must increase. As mentioned in section 2.7, the Eurocodes specifies the weld throat to minimum 3 mm. In these tests the throat thickness of the weld is slightly over 3 mm, which means that a smaller CHS thickness cannot be used unless the plate thickness is changed.

## 9.2 Finite element analysis

The material model used in this FEA is a good approach when modelling with lower strength steel. In this case, when high strength steel is used, the curvature of the material is different which creates a big deviation at the yield point between the nominal values and the true values. In order to minimize this deviation, the properties are calibrated so that they fit the material curve described in section 6.1.2. Even though the material properties are calibrated improvements are necessary.

## 9.3 Experimental work

The experimental work is showing different ways of failure in the connections, which are explained in section 8.2. For specimen CN 1 and CN 3 the failure is very brittle. This type of failure can be severe due to its sudden failure and is therefore hard to foresee. For specimen CN 2 and CN 4 which has the more progressive failure it is easier to see the failure. The failure starts with cracks initiating in the semi-elliptical welds. After the crack initiation the load decreases slightly before starting increasing again. This type of failure is more preferable because total failure can be avoided. The downside with the progressive failure in these tests is that the ultimate load is much lower than the connections with the brittle failure. In order to obtain a higher ultimate load for these connections larger plate dimensions has to be used, resulting in a higher material costs.

When considering the thickness of the CHS, the experimental results confirms the results from the FEA that a smaller thickness can be used. The results from both tests shows that the CHS does not reach critical stress and strain values. Therefore it is interesting to decrease the thickness of the CHS in order to find a critical thickness. This statement is based on the connection failure not the capacity of the CHS itself.

Also showed in section 8.2 fracture occurred at an earlier stage in specimen CN 2 than in specimen CN 4, even though the bevelling angle was smaller in CN 2. In all of the other comparisons it was seen that a smaller bevelling angle gave a higher ultimate load. In order to draw more accurate conclusions more tests have to be performed.

## 9.4 Comparison between FEA and experimental tests

An exact comparison between the FEA and the experimental tests is hard to make. For specimen CN 1 and CN 3, in the FEA, there is a possibility of a higher ultimate load. As mentioned in section 8.2, the inclined plate failed before the welds in specimen CN 1. In figure 42, in annex C, the stresses are distributed along the inclined plate at the position where the specimen is fractured during the experimental test. If the ultimate load is taken from this point in the FEA, the ratio between the FEA and the experimental tests decreases. In order to simulate this more accurate, a more complex model has to be created. If fracture is considered it can be seen at which point the connections fail, hence a more accurate ultimate can be obtained.

# 10 CONCLUSIONS

## 10.1 Hand calculation model

The hand calculation model set for the semi elliptical weld cannot be seen as a good approach for the specimens. The calculated active lengths were above the criteria for the specimens with the connecting piece. In order to obtain a more appropriate calculation model, further research is necessary.

## 10.2 Finite element analysis

From the FEA the ultimate loads were obtained for all the specimens. The models were simulated twice, one time with a coarser mesh and one time with a denser mesh. This was done in order to see the changes in ultimate load for different element sizes. The denser mesh gave an ultimate load that was slightly lower than the value obtained from the coarser mesh elements. Due to this it can be assumed that the ultimate load will decrease more if even finer elements are used.

Further shows that the ultimate load will be much higher, in these tests up to 357 %, for the connections with the connecting piece. Thereby it clearly shows the importance of a stiffener at that location.

There can also be concluded that a larger bevelling angle gives a lower ultimate load. For the specimens including the connecting piece, the influence of a smaller angle increases the ultimate strength with 40 %. For the specimens without the connecting piece the ultimate strength increases with 36 %.

## 10.3 Experimental work

In the experimental work a difference result was obtained from each specimen. The ultimate load in the tests was much higher for the specimens with the connecting piece. The tests showed that the difference of the ultimate load can be up to 413 % higher when the connecting piece is present. Due to this the connecting piece can be seen as essential if a higher ultimate load is necessary. Another conclusion from the experimental work is that a smaller bevelling angle gives a higher ultimate load. Comparing the two bevelling angles the ultimate load increases with up to 14 % when the angle is smaller. The dimensions of the CHS's in these experiments were large enough to not sustain any damage.

## 10.4 Answers to the research questions

- *What is the failure mechanism and the behaviour of the weld?*
  The failure mechanism is shear failure in the semi elliptical weld. When tension is applied the weld will fracture along its shear plane. When more load is added after failure the fracture at the weld root will spread along the weld length.

- *What is the load capacity?*
  The load capacity is different between the specimens with and without the connecting plate. The bevelling angle is also a contributing factor of the load capacity. Table 29 and 30 are showing values obtained from the FEA and the experimental tests respectively.

*Table 27 Ultimate load for each specimen received from the FEA.*

| Specimen | Inclination | Connecting plate | Ultimate load (kN) |
|---|---|---|---|
| **CN 1** | 1:2 | Yes | 672.6 |
| **CN 2** | 1:2 | No | 147.1 |
| **CN 3** | 1:1.5 | Yes | 481.1 |
| **CN 4** | 1:1.5 | No | 107.9 |

*Table 28 Ultimate load for each specimen received from the experimental tests.*

| Specimen | Inclination | Connecting plate | Ultimate load (kN) |
|---|---|---|---|
| **CN 1** | 1:2 | Yes | 809.9 |
| **CN 2** | 1:2 | No | 521.7 |
| **CN 3** | 1:1.5 | Yes | 711.8 |
| **CN 4** | 1:1.5 | No | 247.2 |

- *What is the influence of the connecting plate?*
  In the experimental tests the specimens with the connecting piece have at most 413 % higher ultimate load than the ones without it. In the FEA the ultimate load increases with 357 % when the connecting piece is present.

- *What is the influence of the bevelling angle?*
  There is an influence of the bevelling angle, but not as big as the influence of the connecting piece. It can be seen that the ultimate load increases with a larger angle. The specimens with the smaller bevelling angle have at most 40 % higher ultimate load in the FEA. In the experimental tests the smaller bevelling angle gives 14 % higher ultimate load.

## 10.5 Further research

There are many things to investigate more thoroughly in order to obtain a greater knowledge about the addressed connection. In the bullet points below suggestions of further research are presented.

- Further exploration of weld behaviour, bevelling angle and the connecting plate.
- Tube thickness to diameter ratio.
- Can the connection act as a slip resistant connection?

# 11 REFERENCES


[1] G. Martinez-Saucedo and J. Packer, “Slotted end connections to hollow sections,” CIDECT, Toronto, 2006.

[2] P. W. Marshall, Welded Tubular Connections - CHS Trusses, Boca Raton, 1999.

[3] J. Wardenier, Y. Kurobane, J. Packer, G. van der Vegte and X.-L. Zhao, Design guide for circular hollow sections (CHS) under predominantly static loading, LSS Verlag, 2008.

[4] P. Manoleas, E. Koltsakis, M. Veljkovic and L. Cederfeldt, “The crocodile nose connection an aesthetically appealing joint for CHS,” Naples, 2014.

[5] Y. Kurobane, J. Packer, J. Wardenier and N. Yeomans, 9 - Design guide for structural hollow section column connections, Cologne: CIDECT, 2004.

[6] J. Wardenier, J. Packer, X.-L. Zhao and G. van der Vegte, Hollow sections in structural applications, Geneva: CIDECT, 2010.

[7] K.-H. Brensing and B. Sommer, Steel tube and pipe manufacturing processes.

[8] S. Kalpakijan, Manufacturing engineering and technology, Upper Saddle River; London: Prentice Hall; Pearson Education distributor, 2010.

[9] J. Huang and B. Young, “The art of coupon tests,” 2014.

[10] EN 10002-1: Metallic materials - Tensile testing -Part 1: Method of test at ambient temperature, Brussels: European committee for standardization, 2001.

[11] M. Fadden and J. McCormick, “Finite element model of the cyclic bending behavior of hollow structural sections,” 2013.

[12] EN 1993-1-8: Eurocode 3: Design of steel structures - Part 1-8: Design of joints, Brussels: European committee for standardization, 2005.

[13] S. Willibald, J. Packer, G. Martinez-Saucedo and R. Puthli, “Shear lag in slotted gusset plate connections to tubes,” Amsterdam, 2004.

[14] G. Martinez-Saucedo and J. A. Packer, “Static design recommendations for slotted end HSS connections in tension,” 2009.

[15] Swinden Laboratories, “Slotted end connections,” British steel, Roterham, 1992.

[16] S. Willibald, J. Packer and G. Martinez-Saucedo, “Behaviour of gusset plate connections to ends of round and elliptical hollow structural members,” 2006.

[17] T. Ling, X. Zhao, R. Al-Mahaidi and J. Packer, “Investigation of shear lag failure in gusset-plate welded structural steel hollow section connections,” 2006.

[18] “EN 1993-1-12: Eurocode 3 - Design of steel structures -Part 1-12: Additional rules for the extension of EN 1993 up to steel grades S700,” 2007.

[19] B. Johansson and P. Collin, “Eurocode for high strength steel and applications in construction”.

[20] J.-O. Sperle and K. Olsson, “High strength and ultra high strength steels for weight reduction in structural and safety related applications,” Borlänge.

[21] G. L. Kulak, J. W. Fisher and J. H. Struik, Guide to design criteria for bolted and riveted joints, Chicago: American institute of steel construction, Inc., 2001.

[22] C. Heistermann, “Behaviour of pretensioned bolts in friction connections,” Luleå University of Technology, Luleå, 2011.

[23] RUUKKI, 2014. [Online]. Available: http://www.ruukki.com/Steel/Hot-rolled-steels/Structural-steels/Optim-MC.

[24] FUCHS, [Online]. Available: http://www.fuchs-schrauben.de/engframe.htm.

[25] SS-EN 1090-2: Execution of steel structures - Part 2: Technical requirements for steel structures, Stockholm: Swedish Standards Institute, 2011.

[26] Dassault Systemes, “Abaqus 6.13 Documentation,” 2013.

# 12 ANNEX

## A. TENSILE COUPON TESTS

The tensile coupon tests were performed at LTU in the course Advanced Steel Structures.

The steel used in the tests are 4 mm thick OPTIM S650 plates, delivered by RUUKKI in 2014.

*Table 29 - Coupon properties*

| Specimen | Test direction | Width (mm) | Thickness (mm) | Area ($mm^2$) |
|---|---|---|---|---|
| 1 | Parallel | 22,114 | 4,02633 | 89,03833533 |
| 2 | Parallel | 22,1586667 | 4,01733 | 89,01875022 |
| 3 | Perpendicular | 22,1083333 | 4,00067 | 88,44807222 |
| 4 | Perpendicular | 22,1233333 | 4,01533 | 88,83255778 |
| 5 | Perpendicular | 22,1123333 | 4,05233 | 89,60654544 |
| 6 | Parallel | 22,118 | 4,04833 | 89,54103667 |

In the figure below the stress-strain curves for the six tests are shown.

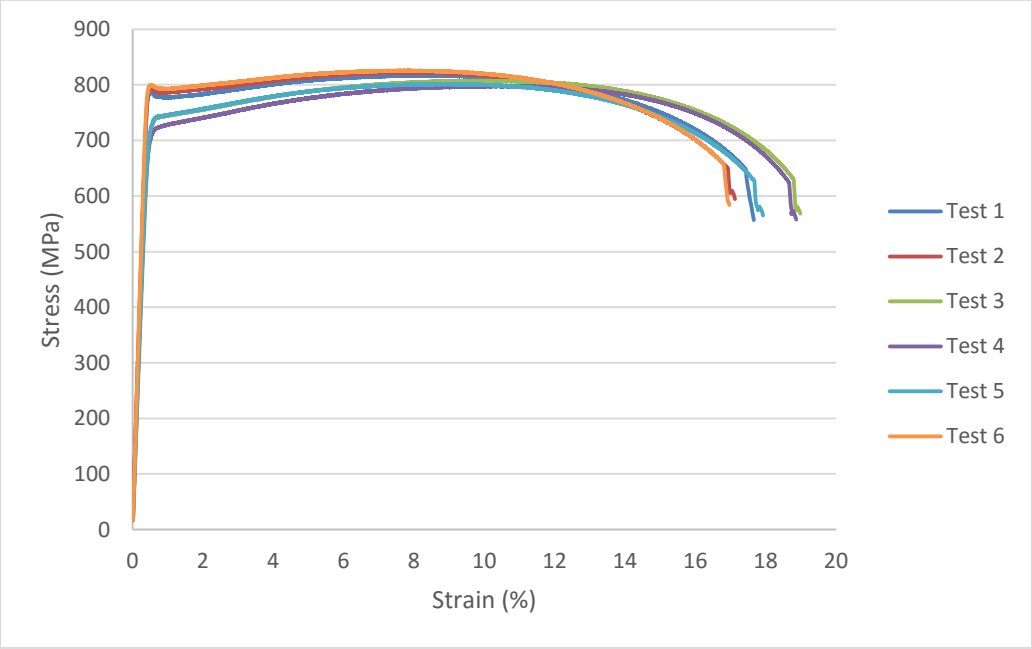


*Figure 37 Stress-strain curves from the tensile coupon test.*

## B. BOLT CALIBRATION

When all the strain gauges were attached in the bolts, they were calibrated. All of the bolts were then, one at the time, tightened in the steel piece shown in figure 35. They were then assembled in the test machine and tested in tension. In the first step a tensile load was applied up to 300 kN where it stayed constant for 300 seconds. After this set the bolt was unloaded with a constant speed. The same procedure was then done twice again, but in these steps the load was only held constant for 30 seconds. Figure 37 and 38 is showing the load versus time and load versus strains respectively.

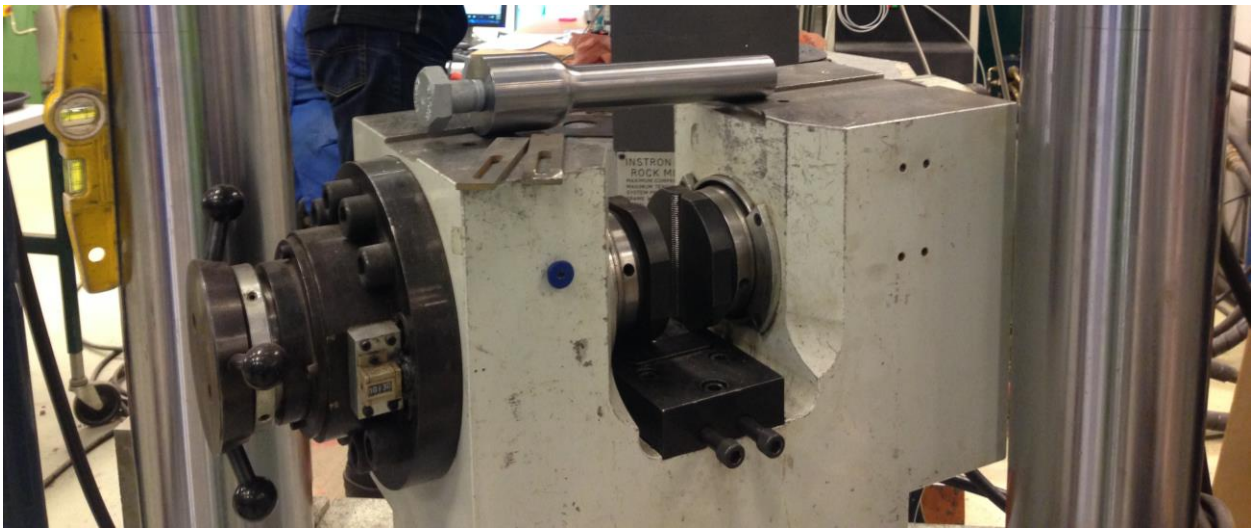

*Figure 38 Bolt mounted in the steel piece which is assembled in the test machine.*

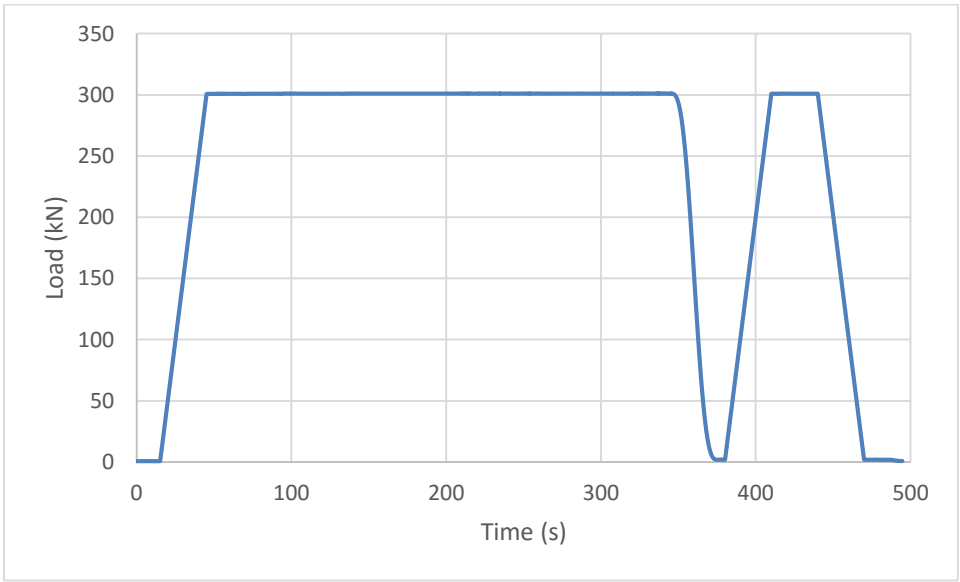


*Figure 39 Calibration for bolt B1.*

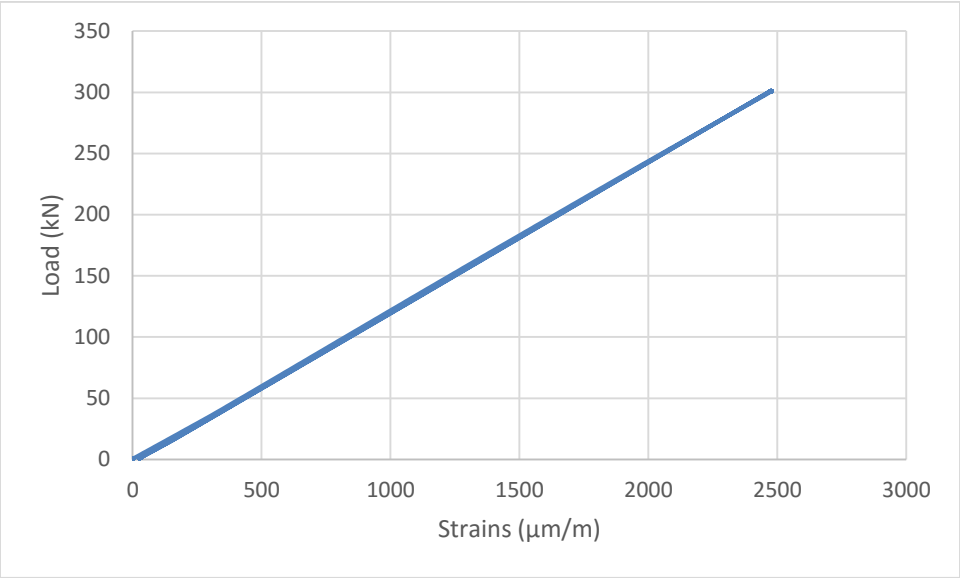


*Figure 40 Load vs displacement for bolt B1.*

## C. VON MISSES STRESSES

In figures 41-48 the von misses stresses in all of the specimens are shown. Two figures are shown for each specimens, where the first figure shows the stresses at the ultimate load and the second shows the stresses at the 3 mm displacement.

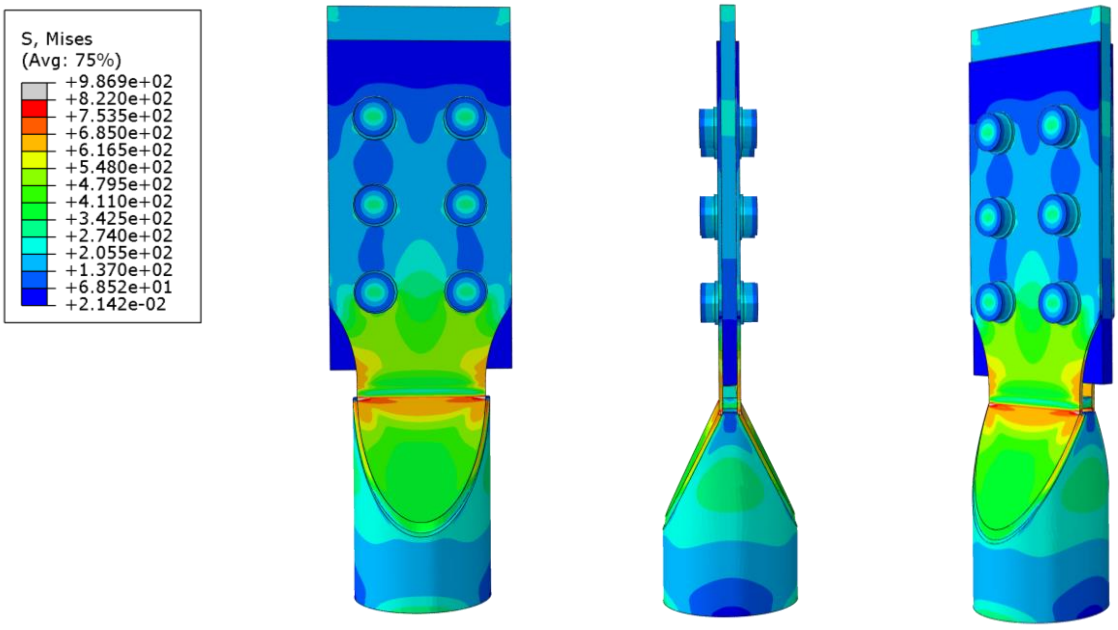


*Figure 41 Stress distribution for specimen CN 1 at its ultimate load.*

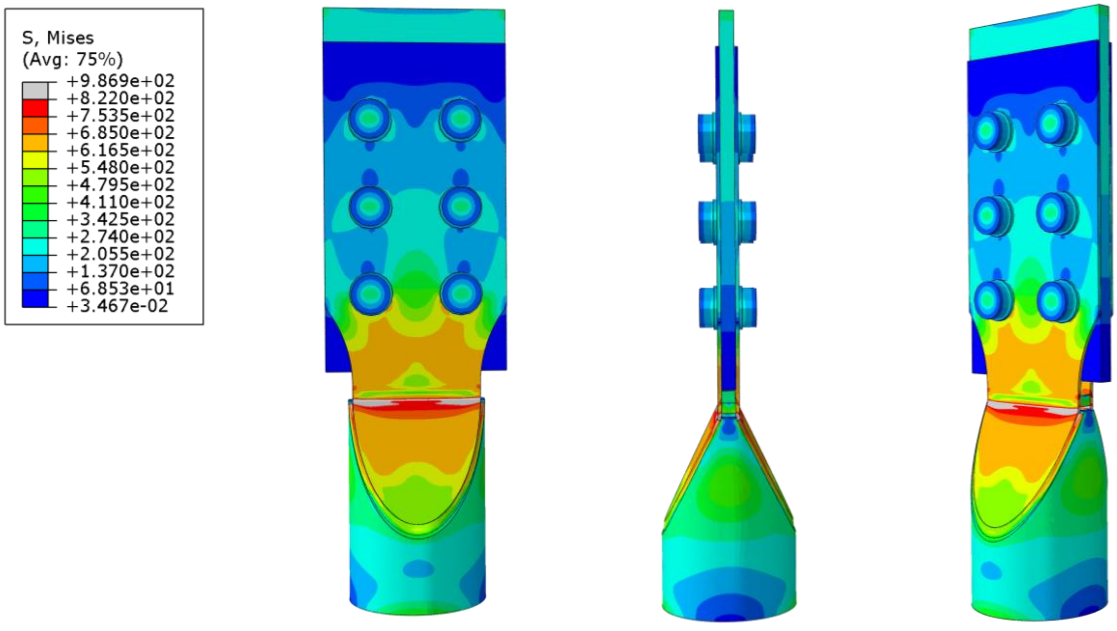


*Figure 42 Stress distribution for specimen CN 1 at the 3 mm displacement.*

As it can be seen in figure 27, the stresses are distributed across the inclined plates. At these points fracture occurs since the tensile strength of the steel plates is surpassed.

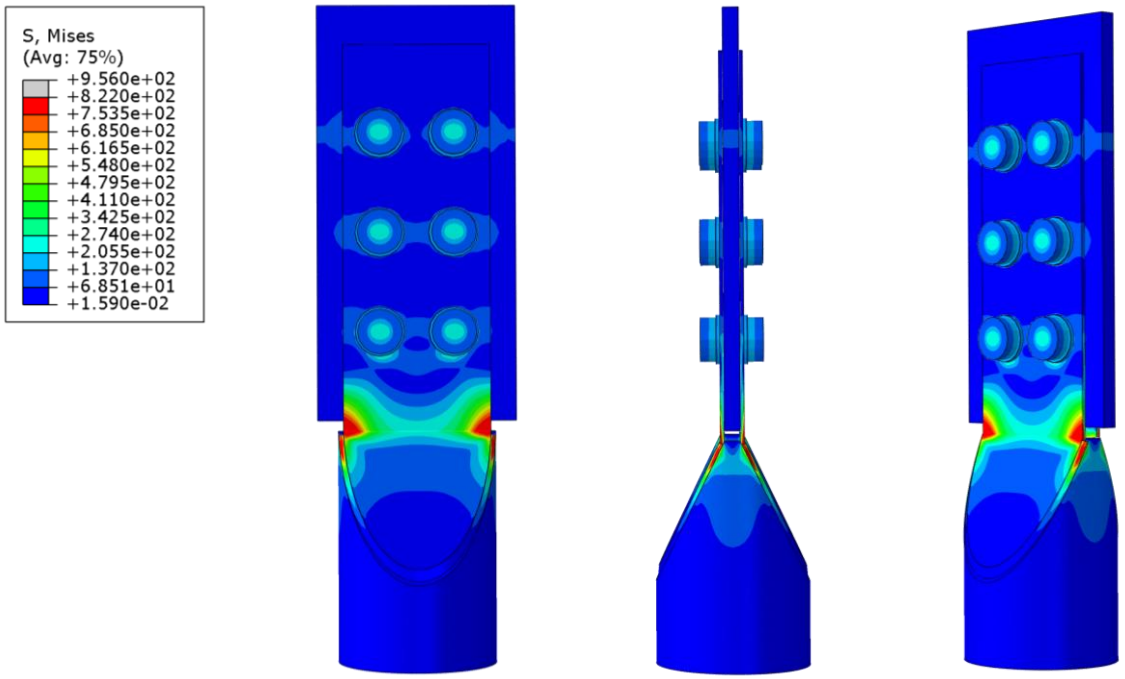


*Figure 43 Stress distribution for specimen CN 2 at its ultimate load.*

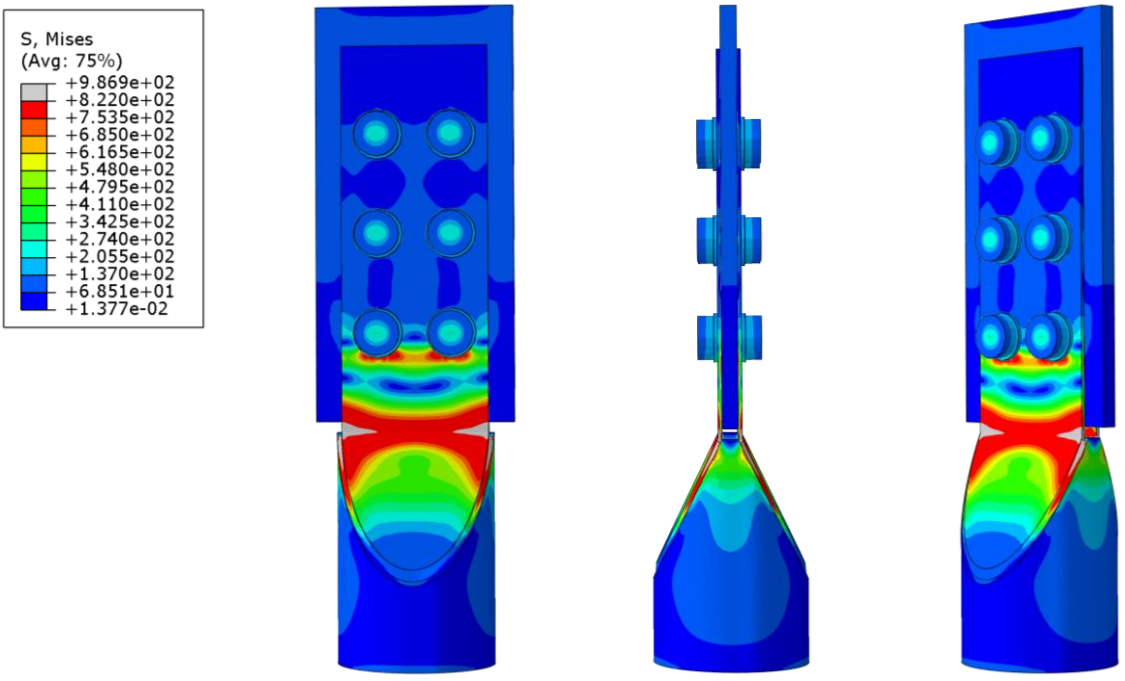

*Figure 44 Stress distribution for specimen CN 2 at the 3 mm displacement.*

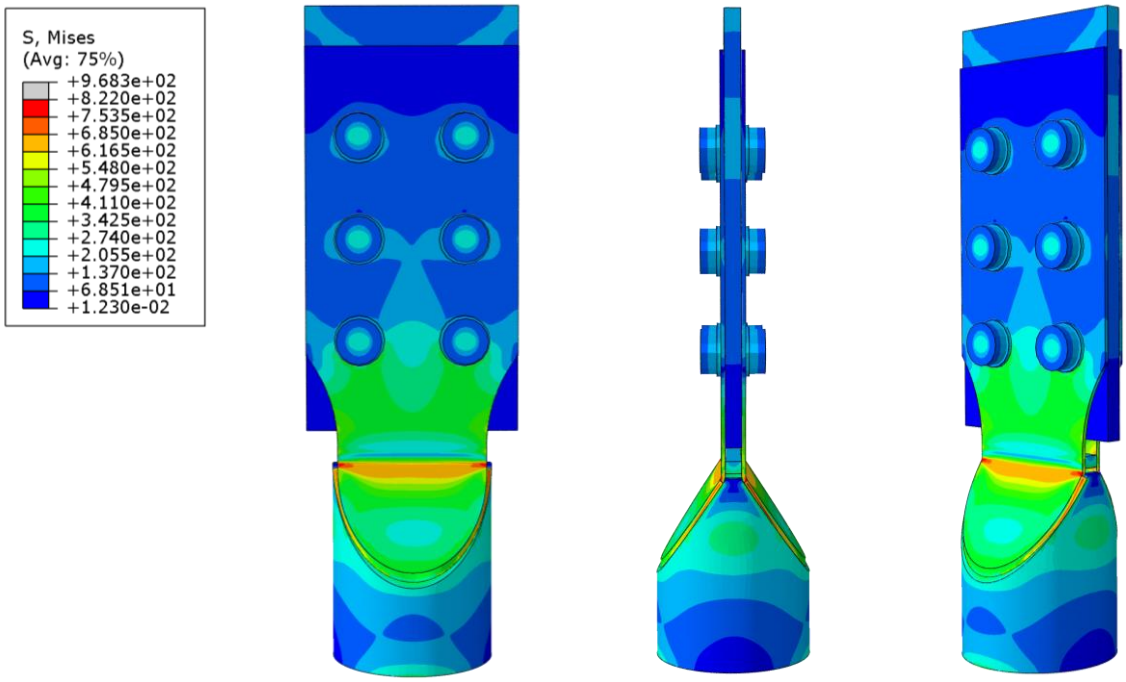


*Figure 45 Stress distribution for specimen CN 3 at its ultimate load.*

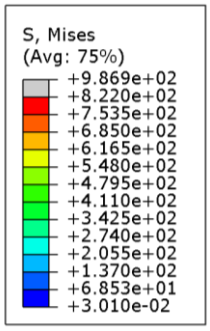

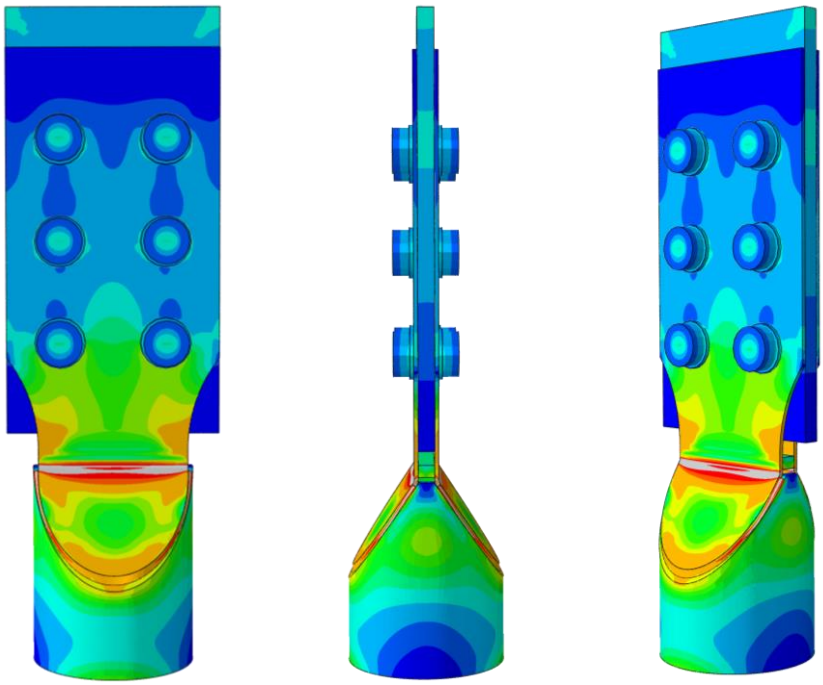

*Figure 46 Stress distribution for specimen CN 3 at the 3 mm displacement*

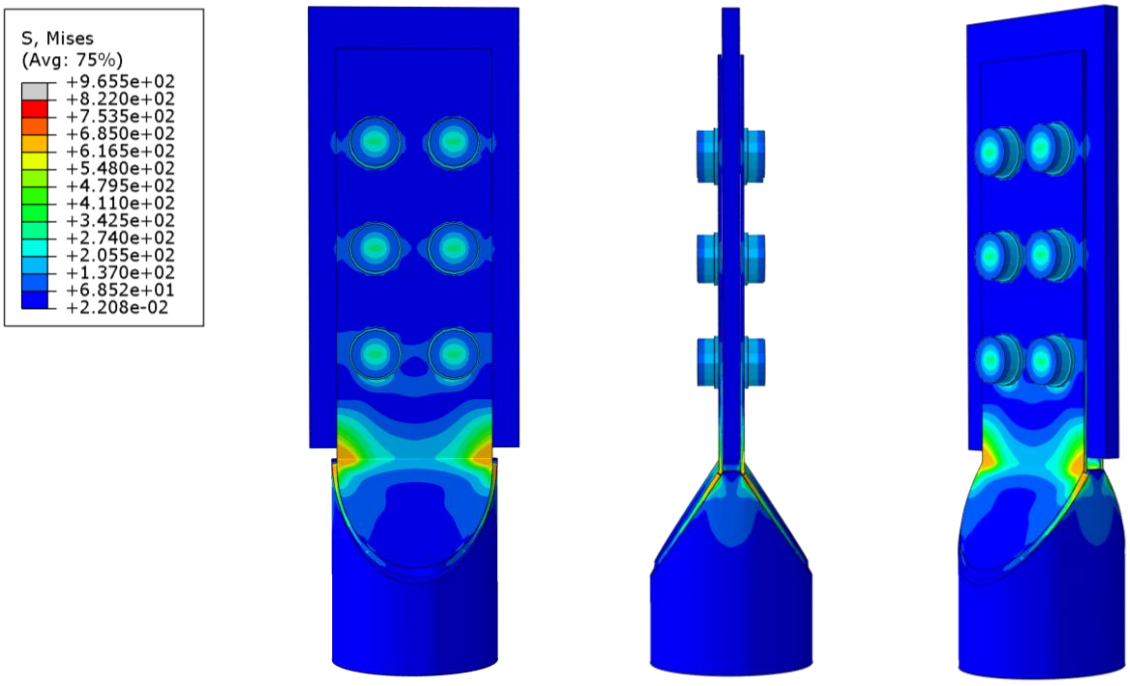


*Figure 47 Stress distribution for specimen CN 4 at its ultimate load.*

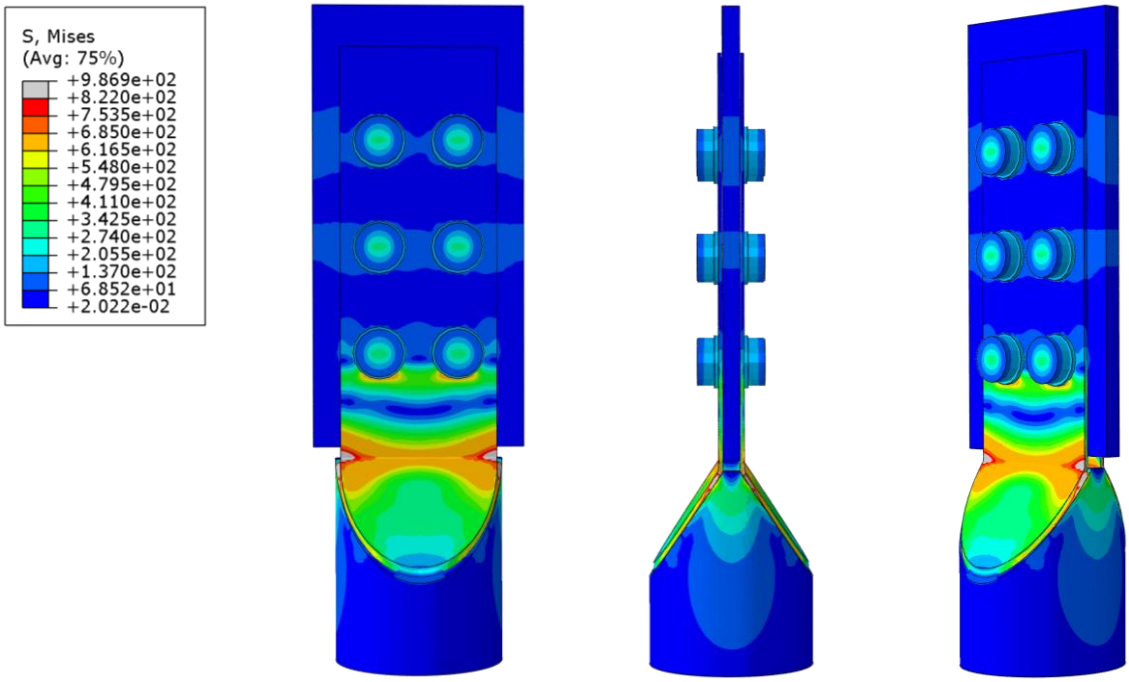


*Figure 48 Stress distribution for specimen CN 4 at the 3 mm displacement*